Two Photon Laser Optogalvanic Spectroscopic Studies of Krypton and Xenon

by

Mushtaq Ahmed

Department of Physics
Quaid-i-Azam University
Isamabad, Pakistan

1997

This work is submitted as a thesis
in partial fulfilment of the
the requirements for the degree of

DOCTOR OF PHILOSOPHY
in
PHYSICS

Department of Physics
Quaid-i-Azam University
Isamabad, Pakistan

CERTIFICATE

It is certified that the work contained in this dissertation is carried out and completed under our supervision.

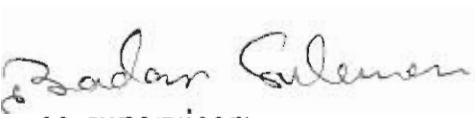

co-supervisor:
Dr. Badar Suleman
Principal Scientific Officer,
Optics Laboratories,
P.O. Box 1021,
Isamabad, Pakistan.

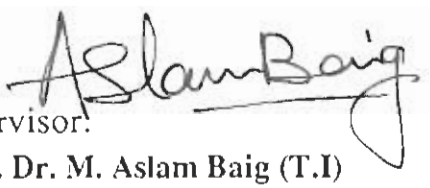

Supervisor:
Prof. Dr. M. Aslam Baig (T.I)
Atomic and Molecular Physics Laboratory,
Department of Physics,
Quaid -i- Azam University,
Islamabad, Pakistan.

Submitted through:

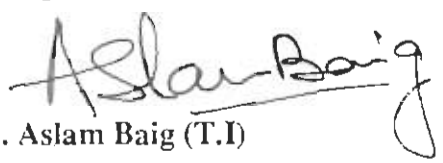

Prof. Dr. M. Aslam Baig (T.I)
Chairman,
Department of Physics,
Quaid-i - Azam University,
Islamabad, Pakistan.

Dedicated to my parents

CONTENTS

Acknowledgement

I acknowledge my gratitude and obligation to my eminent supervisor Prof. Dr. M. Aslam Baig for the guidance, valuable instructions and encouragement through out my research work. I always found him kind, friendly and ever helping.

I express my deep gratitude and obligation to Dr. Badar Suleman for the immense encouragement and constructive guidelines. I recognise his valuable suggestions, comments and professional criticism that played a key role in completing this dissertation. I always found him kind and ever helping.

I am highly grateful to Dr. Shaukat Hameed Khan, Head Optics Labs. Islamabad, for encouraging me to accomplish this work.

I wish to thank my colleagues Dr. Mubeen, Aslam Zia and N. K Piracha for valuable suggestions to complete the thesis. I also wish to thank my other colleagues Dr. Masroor Ikram, Dr. Tahira, Dr. Ghazanfer, Abid Ali and Saleem Ahmed for their being friendly and helping.

Last but not the least, I am indebted to my family for their love, understanding and patience.

ABSTRACT

We report extensive new data on the odd parity Rydberg series of krypton and xenon using single colour two photon laser optogalvanic spectroscopy. In krypton the odd parity bound and autoionized Rydberg series are excited from the $4p^5 5s[3/2]_2$ and $4p^5 5s'[1/2]_0$ metastable levels respectively. A total ten odd parity $4p^5 nd[1/2]_{0,1}$, $4p^5 nd[3/2]_2$, $4p^5 nd[5/2]_{2,3}$, $4p^5 nd[7/2]_{3,4}$, $4p^5 ns[3/2]_2$, $4p^5 ns'[1/2]_0$ and unresolved $4p^5 nd'[3/2]_2$ (or $4p^5 nd'[5/2]_2$) Rydberg series are observed. The $4p^5 nd[1/2]_0$, $4p^5 nd[7/2]_4$, $4p^5 nd'[3/2]_2$ or $4p^5 nd'[5/2]_2$ and $4p^5 ns'[1/2]_0$ series for high n values are reported for the first time. The $4p^5 nd[1/2]_0$, $4p^5 nd[7/2]_4$, $4p^5 ns[3/2]_2$, $4p^5 nd'[3/2]_2$ or $(4p^5 nd'[5/2]_2)$ and $4p^5 ns'[1/2]_0$ Rydberg series have been observed up to n = 23, 49, 44, 39 and 36 respectively. The interchannel interaction among the overlapping Rydberg series has been studied using the multichannel quantum defect theory for J = 0, 2 and 3. In addition, the two photon parity forbidden Rydberg series $4p^5 np[1/2]_1$ excited from the $4p^5 5s[3/2]_2$ level is also observed.

In xenon the odd parity bound Rydberg series are excited from the $5p^5 6s[3/2]_2$ metastable level. A total of eight odd parity $5p^5 nd[1/2]_{0,1}$, $5p^5 nd[3/2]_2$, $4p^5 nd[5/2]_{2,3}$, $5p^5 nd[7/2]_{3,4}$ and $5p^5 ns[3/2]_2$ Rydberg series are observed. The $5p^5 nd[1/2]_0$, $5p^5 nd[7/2]_4$ and $5p^5 ns[3/2]_2$ series for high n values are reported for the first time. The $5p^5 nd[1/2]_0$, $5p^5 nd[7/2]_4$ and $5p^5 ns[3/2]_2$ series have been observed up to n = 21, 47 and 44. We have also observed an even parity (two photon parity forbidden) $5p^5 np[5/2]_2$ Rydberg series excited from the $5p^5 6s[3/2]_2$ metastable level. The multichannel quantum defect theory analysis for the odd parity bound levels of J = 0, 2 and 3 has been performed. Besides the two photon Rydberg series we have also observed a number of one photon transitions excited from the $5p^5 5d$ configuration in the reported spectral region. Some of them can be grouped into $5p^5 nf$ Rydberg series. The $5p^5 nf$ series have been observed up to n = 31.

List of Publications

1. Two Photon Laser Optogalvanic Spectroscopy of the Odd Parity Rydberg series of Krypton.
   Ahmed M, Zia M. A, Baig M. A and Suleman B
   J. Phys. B: At. Mol. OPt. Phys. (1997), 30 (2155)
2. Laser Optogalvanic Spectroscopic Studies of Xenon.
   Ahmed M, Baig M. A and Suleman B
   J. Phys. B: At. Mol. Opt. Phys. (1997) (Submitted for Publication).
3. Multichannel Quantum Defect Theory of the Two Photon Excited Autoionized Rydberg series of krypton.
   (To be published)

Conferences

1. Laser Optogalvanic Studies of $2s\ ^1S \rightarrow np\ ^1P$ Rydberg Series of Atomic heluim.
   Ahmed M and Suleman B
   91 International Workshop on Lasers and lasers Applications (91 IWLLA) in Shanghai China.

2. Laser induced Flurescence Spectroscopy of the $B^3\Pi(o^+_u) \rightarrow X\Sigma^+_g$) System and Two Photon Excitation of E- state of the Iodine Molecule.
   Ahmed M and Suleman B
   91 International Workshop on Lasers and lasers Applications (91 IWLLA) in Shanghai China.

CHAPTER - 1

INTRODUCTION

1.1- Rydberg Atoms

Rydberg atoms have been studied quantitatively since the beginning of atomic spectroscopy (White 1934). The Rydberg atom is simply a Bohr (1913) atom in which an electron is moving classically in a circular orbit around an ionic core. The Rydberg atoms, due to their interesting properties have become a topic of great interest in the field of spectroscopy (Stebbings and Dunning 1983, Gallagher 1994 and references therein). The properties of the Rydberg atoms, scaling with principle quantum number n, are tabulated as below.

Property	n dependence
Binding energy	n^{-2}
Fine structure interval	n^{-3}
Energy between successive n states	n^{-3}
Orbital radius	n^{2}
Geometrical cross section	n^{4}
Polarizability	n^{7}
Radiative lifetime	n^{3}
Dipole moment	n^{2}

The most interesting aspect of Rydberg atoms is their sensitivity to the external electric, magnetic and radiation fields. Even the modest electric field not only perturb the high Rydberg energy levels but also ionise them. Rydberg atoms exhibit large diamagnetic energy shifts due to their large size and scales as n^4. The most fascinating aspect of Rydberg atoms is that they provide opportunities, due to their exaggerated properties, to

perform experiments that are impossible in other systems i.e. interaction of atoms with radiation field. Outstanding examples are one atom maser (Meschede et al (1985) and two photon maser (Brune et al 1987). The interest in Rydberg atoms is due to their importance in real physical systems especially the interstellar space. They play an important role in astrophysical and laboratory plasmas (Jacobs et al 1976).

1.1.1 Production of Rydberg Atoms

For the production of Rydberg atoms the more likely processes used are electron impact, charge exchange and photoexcitation processes:

$$e^- + A \rightarrow A\, n\ell + e^- \qquad \text{(electron impact process)} \qquad 1.1a$$

$$A^+ + B \rightarrow A\, n\ell + B^+ \qquad \text{(charge exchange process)} \qquad 1.1b$$

$$h\nu + A \rightarrow A\, n\ell \qquad \text{(photoexcitation process)} \qquad 1.1c$$

Besides these individual processes, both the electron impact and photoexcitation processes can be used jointly for very effective production of Rydberg atoms.

1.1.2 Detection of Rydberg Atoms

There are different techniques for the detection of Rydberg atoms. These are absorption (Yoshino and Tanaka 1979), collisional ionization (Gallagher and references therein 1994), field ionisation (Delsart et al 1981a, Cooke and Gallagher 1978), fluorescence (Gallagher and reference therein 1994), photoionisation (Hurst and Panyne 1988) and optogalvanic detection (Delsart et al 1981b , Green et al 1976) techniques. For rare gases, the optogalvanic spectroscopy has proved to be a very important technique, which is explained in section 2.1.

1.2. Structure of Rare Gases

The rare gases belong to the group of atoms which have a closed shell in the ground state configuration, resulting in a $^1S_0$ ground state. This configuration makes the rare gases spectra qualitatively different from the alkali and alkali earth elements. The separation between the ground state and the ionization potential is about 4 eV for alkali and ~ 12-24 ev for rare gases. The rare gases (except He) have an ms^2p^6 closed shell

configuration, therefore singly excited states consist of an electron outside the ionic core which has a double fine structure splitting $^2P_{3/2}$ and $^2P_{1/2}$. Consequently, there are two distinct sets of singly excited series converging to two ionization limits $mp^5\,^2P_{3/2}$ and $mp^5\,^2P_{1/2}$, where m stands for 2, 3, 4 and 5 for neon, argon, krypton and xenon respectively.

Alkali atoms can be easily excited to the first excited state by a single photon of energy ~ 2eV, while for the excitation from the ground state of rare gases, one needs photons of energy ~8-20 eV. This makes the optical excitation of rare gases extremely difficult unless one uses the multiphoton processes. A way to avoid this difficulty is to populate the metastable levels, that are fortunately present in abundance in a rare gas discharge. The photo excitation from these metastable levels can then proceed as that of the alkali atoms. This excitation process for the rare gases forms the core of the present studies.

1.2.1 Coupling Schemes for the Rare Gases

The way in which the angular momenta are coupled in an atom has an important bearing on the structure of the spectra. For the atoms of smaller atomic numbers , the predominant coupling is the LS coupling. In LS coupling scheme the electrostatic interaction between electrons are stronger than the magnetic interaction (spin orbit). The orbital angular momenta ℓ_i (where i = 1 to n) of the electrons are coupled to form the total angular momentum **L**:

$$L = \sum_{i=1}^{N} \ell_i \,. \qquad 1.2$$

The spin angular momentum s_i of each electron coupled to form the total angular momentum **S** :

$$S = \sum_{i=1}^{N} s_i \,. \qquad 1.3$$

The total angular momentum **J** is given by:

$$J = |L \pm S| \,. \qquad 1.4$$

The state in LS coupling scheme is designated by $^{2s+1}L_J$ where 2S+1 is the multiplicity of the state.

In heavy atoms the magnetic interaction is stronger than the electrostatic interaction between the electrons resulting in each electron's spin coupling to its orbital angular momenta namely:

$$\mathbf{j_i} = | \boldsymbol{\ell}_i + \mathbf{s}_i | . \qquad 1.5$$

Each $\mathbf{j_i}$ are then coupled to form **J**, the total angular momenta:

$$J = \sum_i j_i \qquad 1.6$$

This coupling is called **jj** coupling scheme. The states with given values of $\mathbf{j_1}$,$\mathbf{j_2}$ and **J** are denoted by means of $(\mathbf{j_1},\mathbf{j_2})_J$.

Apart from the above mentioned frequently used coupling schemes (LS and jj) the other popular coupling scheme is the intermediate scheme or $J\ell$ coupling scheme (Racah 1942, Cowan 1981,). The energy levels of most of the elements when the optical electron is on average at a greater distance from the electrons of the atomic core are characterized by this scheme. In this scheme the orbital angular momentum ℓ of the excited electron couples with the total angular momentum j_c of the core to give the resultant angular momentum **K**:

$$\mathbf{K} = | j_c \pm \ell | . \qquad 1.7$$

The angular momentum **K** is then weakly coupled with the spin angular momentum s of the Rydberg electron to give the angular momentum **J**:

$$\mathbf{J} = | \mathbf{K} \pm \mathbf{s} | . \qquad 1.8$$

In $j\ell$ coupling scheme the states are denoted as $n\ell[k]_J$.

The rare gases (except He) are most conveniently described by this intermediate coupling scheme. Since there are two states of the ionic core corresponding to two different values of the angular momenta j_c, therefore, there are two distinct sets of the excited states depending on j_c . These sets are generally denoted by $n\ell[k]_J$ (for $j_c = 3/2$) and $n\ell'[k]_J$ (for $j_c = 1/2$) .

As mentioned earlier these set of states have two ionization limits, the first ionization limit $I_{3/2}$ corresponding to $mp^5\ ^2P_{3/2}$ ($j_c = 3/2$) configuration and the second ionization limit $I_{1/2}$ corresponding to $mp^5\ ^2P_{1/2}$ ($j_c = 1/2$) configuration.

1.3 Previous Work

Since the pioneering work of Beulter (1935) on the spectroscopic studies of the rare gases and subsequent studies by Yoshino and cowarkers (1970, 1979 and 1985), the topic is still pursued actively using laser spectroscopic techniques (Yoon and Glab 1994, Bounakhla et al 1993, Audouard et al 1990, Pellarin et al 1988). This is partly due to the success of the multichannel quantum defect theory (MQDT) in explaining the interactions among the Rydberg spectra. The Rydberg series below the first ionization limit $I_{3/2}$ overlap and interact with each other resulting in a perturbed structure. Above the first ionization limit these Rydberg levels autoionize into the adjacent continuum (Beulter 1935, Fano 1961, Klar et al 1992, Landais et al 1995).

The J = 1 odd parity Rydberg series of the rare gases are accessible from the ground state using conventional photoabsoption or photoionization (Berkowitz 1979 and references therein, Yoshino and Tanaka 1979, Yoshino and Freeman 1985 and Baig and Connerade 1984) and laser spectroscopy (Demtroder 1981, Gallaghar 1994 and reference therein, Bonin et al 1985, Harth et al 1985). Multi-photon absorption spectroscopy (Wynne and Hermann 1979, Bradley et al 1973 and Nagvi et al 1981) and electron impact spectroscopy (Cederquist and Mannervik 1982) have been used for the investigation of autoionizing phenomenon. Optogalvanic spectroscopy (Green et al 1976, Bridges 1978, Camus et al 1979) and metastable beam spectroscopy (Stebbings et al 1975, Delsart et al 1981, and Knight and Wang 1985) are other powerful tools for the study of high Rydberg series of rare gases.

The odd parity high Rydberg series of krypton have been extensively studied by Yoshino and Tanaka (1979), Delsart et al (1981a,b), and Yoon and Glab (1994). Aymar et al (1981) analyzed the available data on odd parity states for J = 0, 1, 2, 3 by means of MQDT and theoretically simulated the odd parity spectrum of krypton. For xenon the detailed previous studies of the odd parity high Rydberg series have been reported by (Labastie et al 1982, Yoshino and Freeman 1985 , Wang and Knight 1986). Labastie et al (1982) observed the $5p^5ns$ and $5p^5nd$ Rydberg series for J = 0, 1, 2, 3 and 4 excited from $5p^56p$ levels using laser optogalvanic detection in a r.f. discharge of xenon. Lu (1971)

performed the MQDT analysis for odd parity states using the data available in the AEL tables (Moore 1958).

1.4 Present Work

In the present work we have adopted the optogalvanic spectroscopy due to its simplicity and easy detection as compared to other techniques. The presence of high density metastable and semi-metastable states in the discharge provide an easy access to the high Rydberg states and consequently laser excitation to higher J value levels. The first excited multiplet of the rare gases (except He) above the ground state has a mp^5 (m+1)s configuration. This gives rise to four levels, namely $mp^5(m+1)s[3/2]_{2,1}$ and $mp^5(m+1)s'[1/2]_{0,1}$. Two photon laser optogalvanic (LOG) excitation from the $4p^5(m+1)s[3/2]_{2,1}$ and $4p^5(m+1)s'[1/2]_{0,1}$ levels provide an excellent alternative to study the odd parity Rydberg series for all the J = 0, 1, 2, 3 and 4 values due to selection rules $\Delta J = 0, \pm 1, \pm 2$.

The observed series on krypton can be grouped into a total of ten odd parity Rydberg series. Out of the ten, eight series converge to the first ionization limit $4p^5(^2p_{3/2})$. These are $4p^5nd[1/2]_0$, $4p^5nd[1/2]_1$, $4p^5nd[3/2]_2$, $4p^5nd[7/2]_4$, $4p^5nd[7/2]_3$, $4p^5nd[5/2]_2$, $4p^5nd[5/2]_3$, $4p^5ns[3/2]_2$. The rest of the two series namely $4p^5ns'[1/2]_0$ and unresolved $4p^5nd'[3/2]_2$ or $4p^5nd'[5/2]_2$ converge to the second ionization limit $4p^5(^2p_{1/2})$. The $4p^5nd[1/2]_0$, $4p^5nd[7/2]_4$, $4p^5nd'[3/2]_2$ or $4p^5nd'[5/2]_2$ and $4p^5ns'[1/2]_0$ series for high n values are reported for the first time. We have also tried to fill the existing gap between the energy values of Moore (1952) and that of Delsart et al (1981a,b).

For xenon the observed data can be grouped into a total of eight odd parity Rydberg series. These are $5p^5nd[1/2]_{0,1}$, $5p^5nd[3/2]_2$, $5p^5nd[7/2]_{3,4}$, $5p^5nd[5/2]_{2,3}$ and $5p^5ns[3/2]_2$. The $5p^5nd[1/2]_0$, $5p^5nd[7/2]_4$, and $5p^5ns[3/2]_2$ series up to higher n values are reported for the first time. Besides the two photon allowed Rydberg series we have also observed a number of new one photon transitions excited from $5p^55d$ configuration in the reported spectral region. Some of them can be grouped into two $5p^5nf$ Rydberg series.

The interchannel interaction among the overlapping series have been studied using the MQDT analysis for J = 0, 2 and 3 for both krypton and xenon.

Another interesting feature of our study of krypton is the observation of an even parity Rydberg series $4p^5np[1/2]_1$, which is due to two photon parity forbidden transitions. Similarly a two photon parity forbidden series $5p^5np[5/2]_2$ has been observed in xenon. In addition we have observed one photon parity forbidden transitions in xenon. These are $5p^56s[3/2]_2 \rightarrow 5p^55d[5/2]_{2,3}$. Interestingly the single photon parity forbidden transition $5p^56s[3/2]_2 \rightarrow 5p^55d[5/2]_3$ is the strongest one in the entire observed spectra. To the best of our knowledge D.C. discharge laser optogalvanic studies in xenon has been attempted for the first time .

1.5 Lay Out of the Thesis

Chapter two presents briefly the theoretical aspects of discharges, optogalvanic spectroscopy, two photon spectroscopy and multi-channel quantum defect theory . Chapter three describes the experimental set up. Chapter four presents the results and discussion of two photon laser optogalvanic spectroscopy of the odd parity Rydberg series of krypton. Chapter five presents the results and discussion of two photon laser optogalvanic spectroscopy of the odd parity Rydberg series of xenon.

CHAPTER -2

THEORETICAL ASPECTS

2.1 Discharge

The optogalvanic effect, which forms the basis of our present studies, is a result of discharge through gases. The characteristics of discharge significantly change the optogalvanic spectrum. In order to get a better understanding of the optogalvanic effect, a brief discussion of the discharge is attempted bellow.

The subject of the low pressure gas discharge has been studied for a century. A very simple experiment can generate a number of fundamental types of discharges. Figure (2.1) shows the simple arrangement of two metal electrodes connected to a dc power supply inserted into a glass tube. The tube can be evacuated and filled with different gases at various pressures. The minimum sparking potential (V_s) of the d.c. discharge for different gases is different at constant pressure (p) and separation between the electrodes (d). This dependence V_s on pd for various gases is well documented in the literature (Flügge 1956), known as Paschen curves (pd curves).

Figure (2.2) shows a typical V-I characteristic curve for various regimes of the discharge. The first part of the curve describes the regimes where conduction is taking place due to the primary mechanism of spontaneous creation of electron-ion pairs in the plasma. Ionization takes place due to the collective action of the electric field, cosmic rays or many other processes. Near the point D, the voltage drop between the electrodes has reached the breakdown potential V_b of the discharge and we get a glow discharge. In the glow discharge regime, the steady state condition results from the stabilization of a number of coupled processes mainly radiative and electron impact processes. The plasma so formed consists of free electrons, neutral and excited atoms and ions. This plasma presents an internal low impedance which is fixed by the discharge conditions, namely:

1). Nature of the gas,

2). Geometry of the discharge cell, and

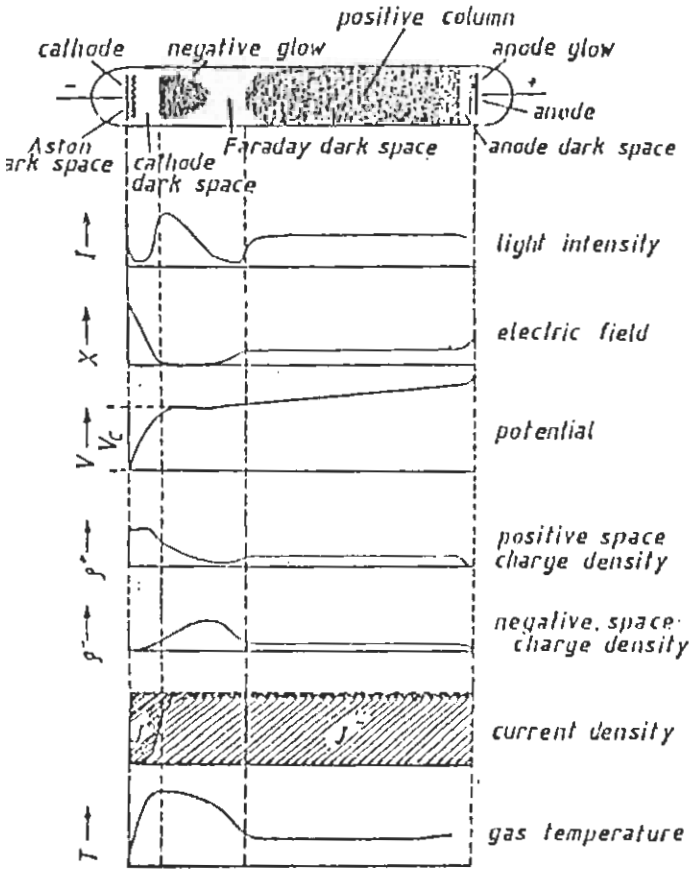

Figure (2.1) Variation of discharge parameters along the length of the discharge.

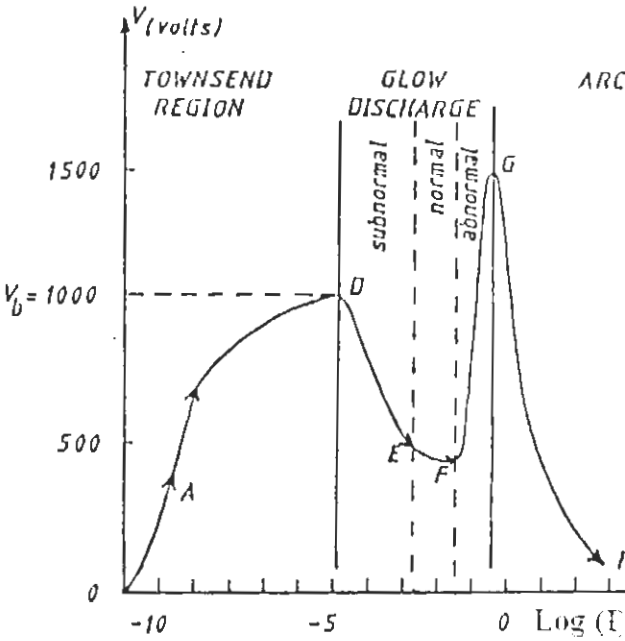

Figure (2.2) V-I characteristic curve for various regimes of the discharge.

3). Dissipation of the electric power in the circuit.

The sensitivity of the optogalvanic signal is limited by the noise which the glow discharge regime generates. In the sub-normal region, conduction takes place due to the secondary emission of electrons by the bombardment of +ve ions on the cathode. The noise spectrum of this regime with average frequency f_i is given by Kopeika and Rosembaum (1976) :

$$f_i = (\mu_i\, p_0/b)\,(T/T_0)\,(\underline{E}/p), \qquad 2.1$$

where μ_i is the ion mobility, p_0 =1 Torr, T_0 =273K , p and T are the gas pressure and temperature, b is the separation between the electrodes and $\underline{E}$ is the average value of the electric field between electrodes.

In the abnormal regime, the cascade ionizing collision and fluctuation of the arrival rate of the electrons at the anode determine the observed noise. The empirical formula for the amplitude of the fluctuations so produce is given by Kopeika (1977) :

$$V_n = \left| 4KT_e + (2p_{dc}\, BR_0/N\nu) \right|^{1/2}, \qquad 2.2$$

where KT_e is the average kinetic energy of the electron, p_{dc} is the average electric power dissipated in the discharge tube, B is the band width of the detector, R_0 is the equivalent resistance of the discharge, N the total number of the free electrons and ν is the elastic collision frequency.

In the normal regime, we observed visibly that the discharge covers only a part of cathode surface. The area covered by the discharge is proportional to the current. This is true what ever the shape of the cathode is.

Kopeika and Rosembaum (1976) mentioned that it is better to work for the spectroscopic measurements in the subnormal regime as compared to the abnormal regime due to increase in sensitivity of optogalvanic detection. According to our experience we get best S/N ratio when the discharge noise is minimum with minimum potential difference at the electrodes. Under these conditions , the discharge is most probably operating in the normal glow regime.

A normal glow discharge is characterised by number of distinct regions. The four major regions are cathode dark space, negative glow, Faraday dark space and positive column. These regions are shown in figure (2.1).

The cathode fall region is the most essential part of the discharge. The maximum potential drop between the electrodes occurs across the cathode dark space. This region is between the cathode and the negative glow. The properties of this region are independent of other regions. Electrons leaving the cathode are accelerated in the cathode dark space and subsequently excite and ionise the gas. Photons, excited and neutral atoms and ions hit the cathode and eject the secondary electrons.

The positive column is very near to the anode. It has a colour characteristic of the gas. Its properties are almost independent of the length of the column. This column closes electric circuit in space between the cathode layer and anode.

The negative glow region is the most important region for the spectroscopic studies. This region is almost field free region and the electric field perturbation to the atomic states (Stark effect) is negligible. Therefore, this region is ideal for the study of the high Rydberg states, which are very prone to perturbation. The length of the negative glow region depends on the geometry of cathode. The hollow cathode shape provides a lengthy negative glow region as compared to plane cathode. This is one of the reason that the hollow cathodes are preferred for the spectroscopic measurements.

The steady state current in a discharge is the result of ionization and recombination. There are a number of mechanisms responsible for the excitation and ionization process. Some are listed as follows:

1) **Electron Impact Ionization**:

An atom in the ground state can get ionized while colliding with an electron depending on the kinetic energy of the electron. This process can be written in the following form:

$$e^- + A \rightarrow A^+ + 2e^-$$

This ionization process can also take place in two-step or multi-step. In these processes first the atom is excited to metastable state by the electron collision and then next electron collision ionizes it.

$$e^- + A \rightarrow A^* + e^-, \qquad e^- + A^* \rightarrow A^+ + 2e^-$$

The metastable produced by the electron impact excitation process provides an easy way to access the high Rydberg states using light sources. In the present studies we

have used the laser to observe the high Rydberg states of rare gases excited from the metastable states.

2) **Metastable- Metastable Collisional Ionization:**

This process plays an important role for the study of the optogalvanic effect. This process has the following form.

$A^* + A^* \rightarrow A + A^+ + e^-$.

3) **Associated Ionization:**

This is a two body collision between a ground state atom and an excited state atom which forms a molecular ion and a free electron.

$A + A^* \rightarrow A_2^+ + e^-$.

2.2 Optogalvanic Spectroscopy

Optogalvanic (OG) effect studies in ionized gases have opened the new possibilities for atomic and molecular spectroscopy, especially Rydberg and refractory materials spectroscopy. Plasma diagnostics, studies of high temperature systems, optical pumping, laser calibration and frequency locking etc are the fields where OG effect finds its direct applications.

The principle of this effect is based upon changes of electrical impedance of the gas discharges when monochromatic light corresponding to the resonance transitions of atoms or molecules is irradiated in the discharge. This effect is due to changes in the steady state populations of various states and hence the related changes in the ionization. The pioneer workers Foote and Mohler (1925), and Penning (1928) have studied optogalvanic effect in two very different types of low pressure discharges. Foote and Mohler (1925) reported this effect in a thermionic diode exhibiting space charge amplification in a cesium vapour. Penning (1928) observed this effect as an impedance increase in a neon discharge while irradiating with a second neon discharge.

There are two basic different mechanisms of optogalvanic effect. (i) Photo excitation of the atoms to higher states increases the probability of impact ionization and hence conductivity of the gas discharge increases or electrical impedance decreases. (ii) Photo excitation of atoms or molecules to higher states perturbs the equilibrium hold

between the electron temperature and the atomic excitation temperature. The energy supplied to the atom by the laser radiation changes the electron excitation temperature, which is reflected as changes in the electron temperature via collisions.

In a hollow cathode discharge, the electron temperature mechanism seems to dominate the OG effect. The experimental evidences in support of this mechanism are:

I) The OG efficiency is independent of the ionization potential (Keller and Zalewski 1982).

II) The OG efficiency is independent of the energy deference between the laser excited energy level and the ionization potential (Keller et al 1979).

III) The increases in the electron temperature due to the increases in atomic emission intensity have been observed by Dreze et al (1982).

Of course both mechanisms proceed simultaneously and at different discharge conditions and for different excitations, one may dominate the other. These two mechanisms are discussed in detail by Keller et al (1983).

Figure (2.3) shows the various types of gas discharges used for optogalvanic spectroscopy. Both D.C. and A.C. (radio frequency) discharges are used. Foote and Mohler (1925) reported this effect in a thermionic diode exhibiting space charge amplification in a cesium vapour. Penning (1928) observed this effect as an increase of the impedance in a neon discharge while irradiating with a second neon discharge. OG spectroscopy with radio frequency (r.f) discharge has an advantage over d.c discharge that the noise caused by the sputtering can be avoided. Low pressure r.f. discharge plasma is highly homogeneous and has a relatively high electron temperature. The weaker the background ionizations, the higher the S/N ratio.

Despite of the long history, optogalvanic effect emerged as a powerful spectroscopic tool with the advent of tunable lasers. Green et al (1976) observed optogalvanic effect in neon hollow cathode using a C.W. dye laser. Since the work of Green et al (1976) optogalvanic research and its applications is rapidly expanding in different types of spectroscopy. Shuker et al (1983), and Lawler and Doughtly (1983) have discussed the theoretical and experimental aspects of optogalvanic effects in neon discharge.

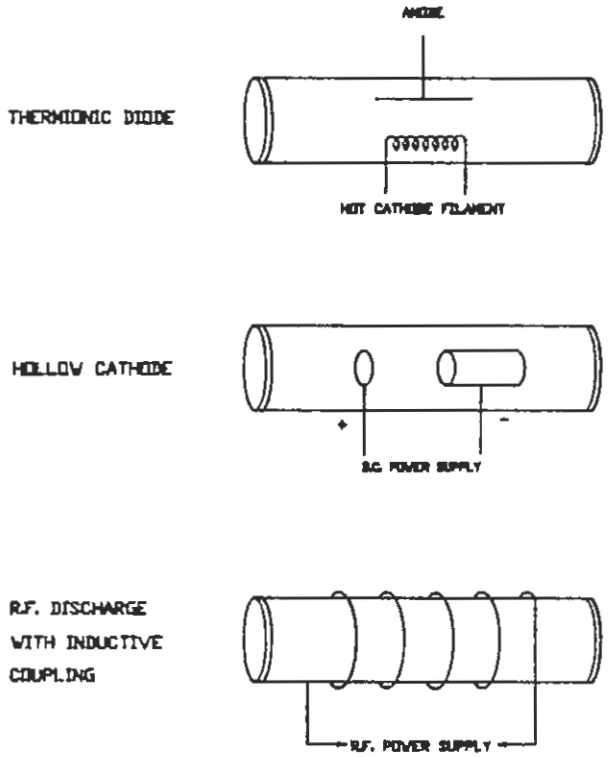

Figure (2.3) Various gas discharge plasma for optogalvanic spectroscopy.

The easy detection and high sensitivity of laser optogalvanic (LOG) effect has offered a variety of applications for laser spectroscopy (Camus 1983, Glodsmith and Lawler 1981). This effect is very efficient in the detection of trace elements (Turk et al 1979). In hollow cathode discharges, the refractory elements are sputtered in to the gas phase due to the positive ions collisions with cathode and their spectra is studied by simultaneously irradiating with the lasers. The LOG effect can be used as a diagnostic tool for the study of low energy plasmas (Ganguly and Garscadden 1985). LOG spectroscopy has been extensively applied for the study of Rydberg atoms (Barbieri et al 1990 and references therein). Another advantage of LOG effect is an accurate wavelength calibration of the tunable dye lasers in any spectral region (Hippler and Pfab 1993).

There are number of advantages and disadvantages of optogalvanic detection which are as follows:

Advantages

i) The main advantage of this effect is a non-optical detection of an optical transition.

ii) 4π solid angle detection.

iii) Slow transient signal with pulse laser excitation.

iv) Almost independent of wavelength scale.

v) No background from the scattered excitation laser light.

Disadvantages

I) Low noise level limited by the sputtering in the hollow cathode lamps.

ii) Sensitivity to r.f. noises.

iii) Time delay limited by the circuit feeding the discharge.

iv) Non linearity of the signal depending on position of the laser beam in the discharge between the electrodes and from the discharge conditions.

v) Presence of the residual electric field causing shifts and broadening in energy levels.

2.3 Two Photon Spectroscopy

Multiphoton spectroscopy is a useful technique for the study of the excited states in atoms and molecules. This technique permits to get information on states lying at two, three or more photon excitation energies using intense light source. This method did not gain popularity due to lack of very intense light sources. The two photon absorption was studied theoretically about seventy years ago (Dirac 1958). The advent of lasers changed the situation drastically. The availability of the intense light sources in the form of lasers resulted into experimental data on multiphoton processes cross sections. The two photon resonances in a gas interacting with a strong radiation field was analysed by Vasilenko et al (1970). Later, a number of studies on high Rydberg states in atoms such as energy levels, fine structure, hyperfine structure, Zeeman effect, Stark effect and collisional mixing have been reported (Bokor et al 1980, Edelstein and Gallagher 1978) using laser multiphoton spectroscopy. The availability of the tunable UV lasers have further pushed the multiphoton excitation process into a new spectral region.

In multiphoton excitations, the two photon absorption is the most commonly used technique. A two photon excitation is quite different from a two step excitation. As an example, we consider a three level system as shown in figure (2.4) and designate the lower level as $|g>$, the intermediate level as $|n>$ and the final level as $|f>$. The parity of the $|g>$

and | f > levels is same and that of the level | n> is different. The excitation from the initial level | g > to the final level | f > can be achieved by a two step absorption (Figure 2.4 a) if:

$$E_{gf} = \hbar\omega_{gn} + \hbar\omega_{nf} . \qquad 2.3$$

Where ω_{ng} and ω_{nf} are frequencies of the two light sources. This two step or two colour technique is used quite often in spectroscopy. Note that each transition from the state | g > to the state | n > and from the state | n > to the state | f > is electric dipole allowed. The method works very well if the pumping rate from the state | g > to the state | n > is higher than the decay rate of the state | n>. The transition probability for two step process can be written as:

$$W \sim |\langle g|z|n\rangle|^2 \bullet |\langle n|z|f\rangle|^2 \quad , \qquad 2.4\ a$$

$$W \sim W_{g\to n} \bullet W_{n\to f} \quad , \qquad 2.4\ b$$

If we use a single intense light source of frequency ω_ℓ , then it is possible to excite the level | f > from the level | g > (Figure 2.4 b), provided :

$$E_{gf} = \hbar\omega_{gn} + \hbar\omega_{nf} = 2\hbar\omega_\ell , \qquad 2.5$$

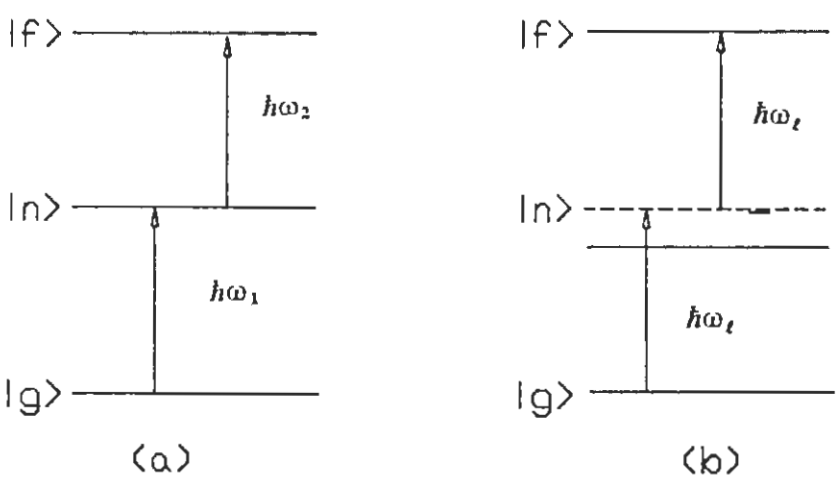

Figure (2.4) Schematic diagram for three level system. (a) The two step absorption; (b) The two photon absorption. The state | g > and the state | f > have the same parity and the state | n > has different parity from that of | g > and | f >.

resulting in a two photon absorption. Two photon excitation can be considered as the simultaneous absorption of two photons. The first one is from the initial state to an intermediate virtual state and the next one is from this intermediate virtual state to the final state.

The transition probability of two photon process is quite different from that of the two step excitation and is generally very weak (being a second order effect). Since the transition probability is very weak therefore, intense optical excitation source is required to investigate the two photon absorption processes. A discussion of two photon transition probability is given below.

2.3.1 Two Photon Transition Probabilities

We consider a fixed atom in a two frequency field, assuming that the energy difference between two states $|g>$ (initial state) and $|f>$ (final state) $E_f - E_g$ is equal to the total energy of two photons $\hbar(\omega_1+\omega_2)$. In this case two quantum atomic transitions $g \rightarrow f$ are possible. The probability of transition per unit time is (Letokhov and Chebotayev 1977):

$$W_{gf} = (2\hbar^4\Gamma)^{-1} |A_{gf}|^2 E_1^2 E_2^2 \quad , \qquad 2.6$$

where A_{gf} is the matrix elements of the two photon transition given by

$$A_{gf} = \sum_n \left[\frac{\langle g|pe_1|n\rangle \langle n|(pe_2|f\rangle}{\omega_{ng} - \omega_1} + \frac{\langle g|pe_2|n\rangle \langle n|(pe_1|f\rangle}{\omega_{ng} - \omega_2} \right], \qquad 2.7$$

where p is the electric dipole operator, e_1 and e_2 are the polarization vectors. The summation is over all intermediate states $|n>$ including continuum and $\Gamma = \Gamma_{gf}$ is the half width at half maxima for the $|g> \rightarrow |f>$ transition.

These equations can be derived directly from the perturbation theory (Dirac 1958). The equations (2.6) and (2.7) are written for a simple case in which the states $|f>$ and $|g>$ are nondegenerate and all the intermediate states $|n>$ are far from resonance i.e.

$$|\omega_{ng} - \omega_1| >> \Gamma_{gf} \ .$$

It is also assumed that the rate of the two photon transitions is much less than the relaxation rate of the final state $|f>$, so that effects of two photon transition saturation may be neglected.

The appearance of the intermediate states in the above formula reflects the possibility of attaining the final state via series of intermediate states, which are connected with the initial and final states by non zero matrix elements. In each transition the system absorbs or emits one photon. The transition $|g\rangle \rightarrow |f\rangle$ is, therefore, a two photon process. It must be emphasised here, that this transition cannot , in principle, be divided into a temporal sequence of events. It should be understood that both photons are absorbed simultaneously. It would be incorrect to assume that first one photon is absorbed and then the other one. In such a case the transition would be equivalent to two single photon transitions.

In our experiment we are using single focused laser beam of frequency ω_L , therefore,

$$\omega_1 = \omega_2 = \omega_L ,$$

The transition probability then becomes:

$$W_{gf} = \frac{E^4}{2\hbar^4\Gamma}\left|\sum_n \frac{\langle g|pe|n\rangle\langle n|pe|f\rangle}{\omega_{ng} - \omega_L}\right|^2 . \qquad 2.8$$

The transitions are Doppler broadened.

The two photon transition probability for the inert gases:

The energy denominator in A_{gf} for the expression of the two photon transition probability plays an important role in the two photon absorption cross sections. If a real atomic level lies very close to the virtual level, then the contribution from this single term may exceed from all the other terms in the summation. Such two photon resonant transitions have been observed in alkali metals.

In our studies of inert gases , we did not observe any resonant enhancement throughout the spectral region studied. Therefore, it is more appropriate to choose the truncated basis set (Bebb and Gold 1966, Payne et al 1981) in evaluating the summation in the equations (2.7, 2.8). As discussed by Payne et al (1981), the summation can be replaced by an average contribution coming from each intermediate state. Therefore, A_{gf} for inert gases can be written as:

$$A_{gf} = \beta < g | z^2 | f > \quad , \qquad 2.9$$

where β is a constant. Generally it is determined by experiments.

There are two important features of the two photon absorption:

(i) Two photon absorption occurs between states of the same parity.

(ii) The probability of two photon absorption is proportional to the fourth power of the electric field i.e. to the square of the intensity if both photons are from the same laser.

Two photon transitions are possible only due to the perturbations of the atomic states by a light field. This perturbation acts on both the ground and final atomic levels. Therefore it results in a shift and broadening of the two photon transition and is proportional to the laser power.

In general, the shift of an atomic level induced by an optical field $E=E_0 \cos(\omega t-kz)$ is given by the perturbation theory (Letokhov and Chebotayev 1977, Mizushima 1964) :

$$\Delta E_m = h\delta\nu_m = (\frac{E^2}{4})\sum_n \left[\frac{(P_{nm}e)^2}{E_m - E_n - \hbar\omega} + \frac{(P_{nm}e)^2}{E_m - E_n + \hbar\omega} \right] . \qquad 2.10$$

where summation is over all unperturbed atomic states $| n >$. P_{mn} is the electric dipole matrix elements between the states $| m >$ and $| n >$. Natural damping of the states has been ignored in the above equation hence the above equation is valid as long as 1/h times the energy denominator is larger than the natural line width of the levels.

Equation (2.10) is also true for the two photon transitions. For the initial level the shift is expressed as:

$$\Delta E_g = -\frac{E_1^2}{4\hbar} \sum_n \frac{(Pe_1)_{gn}(Pe_2)_{ng}}{\omega_{ng} - \omega_1} \quad . \qquad 2.11$$

In the case of exact resonance , the term Γ_{ng} (finite width of the transition) should be added to the resonance denominator in equation (2.11).

The shift of the levels caused by the second field should also be allowed. If $\omega_1 = \omega_{ng}$ and $\omega_1 + \omega_2 = \omega_{fg}$ then the second field ω_2 automatically set near resonance with the frequency ω_{fn}. So the power shift for the level $| f >$ have the similar expression as

equation (2.11). Therefore, the two photon resonance shift depends on the sum of the shifts of the initial and final levels (Bloembergn and Levnson 1976).

2.3.2 Parity Forbidden Transitions

As discussed earlier, a two photon transition is allowed only if the initial and the final states have the same parity. In our experiment, we have observed two photon transitions between states of different parity. Single photon parity forbidden transitions have been observed (Ito et al 1993 ,Kellert et al 1980, Huggs et al 1981 and Ernst et al 1988) and are thought of arising from the ℓ mixing of states due to the collisional or electric field perturbation.

In order to calculate the intensity ratios of the forbidden to the allowed transitions, consider a transition from a state $|g>$ to a state $|m>$ such that the parity of state $|m>$ is different from that of state $|f>$. The allowed two photon transition probability is given by equation (2.8). The two photon transition between the state $|g>$ and the state $|m>$, being of different parity, is forbidden. The external perturbation changes the character of the states. In Rydberg atoms the effect is much more pronounced on the final state where n is very large. The perturbative effect on lower state $|g>$ is very small and can be neglected. Then to first order , the perturbed state $|m_p>$ can be written as:

$$|m_p> \rightarrow |m> + \Sigma_i \alpha_i |i> \qquad 2.12$$

where the expansion coefficients α_i have the form:

$$\alpha_i = <i|H'|m> / (E_i - E_m), \qquad 2.13$$

and E_i and E_m are the energies of state $|i>$ and $|m>$.

The matrix element in equation (2.7) can be written in a compact form as:

$$A_{gf} = \Sigma_n <g|pe|n><n|pe|f> / (\omega_{ng} - \omega) \qquad 2.14$$

For a transition from state $|g>$ to a perturbed state $|m_p>$ the matrix elements take the form:

$$A_{gm} = \Sigma_n <g|pe|n><n|pe(|m> + \Sigma_i \alpha_i |i>) / (\omega_{ng} - \omega) \qquad 2.15$$

$$A_{gm} = \Sigma_n ((<g|pe|n><n|pe(|m>) + (<g|pe|n><n|pe|\Sigma_i \alpha_i i>)) / (\omega_{ng} - \omega)$$

The first term in the above equation is zero due to the two photon parity selection rule. Hence

$$A_{gm} = \Sigma_n \; < g \,|\, pe \,|\, n > < n \,|\, pe \,|\, \Sigma_i \; \alpha_i \; i \; > / \; (\; \omega_{ng} - \omega) \qquad 2.16$$

$$A_{gm} = \Sigma_i \; \alpha_i \; \Sigma_n \; < g \,|\, pe \,|\, n > < n \,|\, pe \,|\, i \; > / \; (\; \omega_{ng} - \omega) \qquad 2.17$$

Therefore, the two photon transition probability from state $|\, g >$ to a mixed state $|\, m_p >$ becomes:

$$W(\text{forbidden}) = \frac{E^4}{2\hbar^4 \Gamma} \left| A_{gm} \right|^2 \quad . \qquad 2.18$$

The matrix element of A_{gm} will be non zero if the state $|\, i >$ has the same parity as that of the state $|\, g >$.

The ratio of forbidden to allowed transitions can be written as:

$$\frac{W(\text{forbidden})}{W(\text{allowed})} = \left| \sum_i \alpha_i \frac{\langle g | pe^2 | i \rangle}{\langle g | pe^2 | f \rangle} \right|^2 . \qquad 2.19$$

The α_i's are expansion coefficients (to first order) of a perturbed state. In our experiments, the perturbation comes from the electric field. We have observed two photon parity forbidden transitions from the state $|\, s >$ to the state $|\, p >$. The electric field of the discharge can mix multiplets of the state $|\, s >$ and state $|\, d >$ in a pure state $|\, p >$. The Stark matrix elements in α (equation 2.13) can be easily computed. Generally, the state which lies closer to the state $|\, p >$ causes the maximum contribution in α's and a two photon transition can take place to that level. This appears as a transition, which is otherwise forbidden.

2.4 Multichannel Quantum Defect Theory

Quantum defects are a measure of the difference between energy levels of hydrogenic system and energy levels of many electron atoms. For an electron moving in a pure coulombic potential ($-z / r$) the energy values in atomic units are:

$$E_n = - (z^2)/(2n^2). \qquad 2.20$$

where n is an integer. For a multielectron atom, a Rydberg electron sees an effective potential V(r) having the coulomb form in the limit of large r. The energy values for such an electron may be expressed in term of effective quantum numbers ν_n and is given by:

$$E_n = -(z^2)/(2\nu_n^2), \qquad 2.21$$

and the difference $(n - \nu_n)$ is known as quantum defect μ_n.

Most of the observed Rydberg spectra can be explained by measuring the quantum defect. Generally it has a constant value for a particular Rydberg series. But sometimes one observes strong irregularity in quantum defect and hence in the position of a particular series member. This irregularity is attributed to perturbation of a series due to configuration interaction. The Multichannel quantum defect theory (MQDT) explains quite remarkably this behaviour. In addition MQDT has also addressed the phenomena like autoionization etc. It has gained special significance while explaining the Rydberg spectra of inert gases.

Multichannel quantum defect theory was originally formulated by Seaton (1966). Since than a number of workers have developed different formulation of MQDT. The MQDT theory was not used extensively till Lu and Fano (1970) developed a graphical analysis technique. The quantum defect theory (QDT) can have many forms depending on the basis functions. Two of them are commonly used. One is based on the separated electron and ion and uses **R** matrices (Seaton 1966, 1983), Guisti-Suzor and Fano (1984), Cooke and Cromer (1985), Connerade et al (1985), Ueda (1987) and Baig and Bhatti (1994)). The second is based on the normal modes of the short range electron-ion scattring (Fano (1970), Lu and Fano (1970) and Lee and Lu (1975)). Cooke and Cromer (1985) approach has the advantage of showing the connection between two formulations.

The basic problem is to calculate the wavefunction of the Rydberg atom. To develop the Rydberg atom wavefunctions one can start with the Shrodinger equation for the hydrogen atom:

$$\partial^2\rho/\partial r^2+[2E + 2/r - \ell(\ell + 1)/r^2]\rho = 0, \qquad 2.22$$

where E is the energy and r is the distance of the electron from the proton.

In general, for $r > r_0$, the wave function of the Rydberg state of an atom other than hydrogen can be written as:

$$\psi=\{f(E, \ell, r)\cos(\pi\mu) + g(E, \ell, r)\sin(\pi\mu)\}(1/r), \qquad 2.23$$

for which $\psi \rightarrow 0$ as $r \rightarrow \infty$, gives

$$E = -1/2(n-\mu_\ell)^2, \qquad 2.24$$

where μ_ℓ is known as the quantum defect. The f and g are coulomb functions (Fano 1970 and Seaton 1983)

This wave function is a standing wave obeying the boundary condition that $\psi \rightarrow 0$ as $r \rightarrow \infty$ and ψ is finite at $r = r_0$ and represents Coulomb wave scattering from the ionic core.

Now if the ionic core of the Rydberg atom does not have a single spherically symmetric state then the energy and the angular momentum of the Rydberg electron and ion are not conserved separately and it is possible for a Rydberg electron to exchange energy with the ionic core. As a result, the different combinations of energy, angular momentum and parity of Rydberg electron and ionic core are taken such that the total, energy E (core + electron), the angular momentum J and parity of the atom is conserved.

Each set of bound Rydberg states and associated continuum having same angular momenta J, spin and parity constitute a channel. These channels are called collisional channels and describe a Rydberg electron with an energy 'E_i' and a core in a definite energy configuration . Therefore, the total energy of a collisional channel has two parts, E_i (Rydberg electron energy) and I_i , the core configuration energy (the ionization limit) : $E(\text{total}) = E_i + I_i$. A collisional channel is open if $E_i > 0$ and closed if $E_i < 0$. Far from the ionic core ,the collisional channel wave function can be described by:

$$\phi_i = \{f(E_i, \ell, r)\cos.(\pi\nu_i) + g(E_i, \ell, r)\sin(\pi\nu_i)\}(\chi_i/r) , \quad r > r_0 \qquad 2.25$$

where $\pi\nu_i$ is the phase shift and ν_i describes the fraction of the regular and irregular coulomb function. The χ_i is the product of the total ionic wave function and the angular part of the Rydberg electron wave function including spin wave function. This represent a single incident incoming hydrogenic wave which has undergone a phase shift after scattering from the core. In order to construct a wave function which satisfies the boundary condition near $r = r_0$, we can take the linear combination of the ϕ_i 's after affecting a unitary transformation, which will only introduce a phase shift (Cooke and Cromer 1985):

$$\Psi_\alpha = \sum_i U_{i\alpha}\{f(E_i, \ell, r)\cos.(\pi\mu_\alpha) - g(E_i, \ell, r)\sin(\pi\mu_\alpha)\}(\chi_i/r), \qquad 2.26$$

where $\pi\mu_\alpha$ is the phase shift and $U_{i\alpha}$ is the unitary transformation.

The wave functions Ψ_α are the eigen functions which satisfy the boundary condition at $r = r_0$ but they do not satisfy the boundary condition as $r \rightarrow \infty$. In contrast ϕ_i wave functions satisfy the boundary condition as $r \rightarrow \infty$ but not at $r = r_0$. Generally for $r > r_0$ the wave function Ψ are the linear combination of either Ψ_α or ϕ_i .

$$\Psi = \sum_i A_i \phi_i = \sum_\alpha B_\alpha \Psi_\alpha \qquad 2.27$$

Using equations (2.25, 2.26 and 2.27) yields the Fano (1970) MQDT formulation:

$$A_i = \sum_\alpha U_{i\alpha} B_\alpha \cos\pi(\nu_i + \mu_\alpha), \qquad 2.28a$$

$$0 = \sum_\alpha U_{i\alpha} B_\alpha \sin\pi(\nu_i + \mu_\alpha) . \qquad 2.28b$$

According to Cooke and Cromer (1985) there is another equivalent set of equations having the form:

$$B_\alpha = \sum_i U_{i\alpha} \cos\pi(\nu_i + \mu_\alpha) A_i , \qquad 2.29a$$

$$0 = \sum_i U_{i\alpha} \sin\pi(\nu_i + \mu_\alpha) A_i , \qquad 2.29b$$

The two set of equations (2.28b and 2.29b) yield nontrivial solution only if:

$$\det | U_{i\alpha} \sin\pi(\nu_i + \mu_\alpha) | = 0. \qquad 2.30$$

This relation defines the quantum defect surface. For a two channel problem this equation (2.30) defines a line whereas for N channel problem it defines a N-1 dimensional surface.

An Alternate R Matrix Formulation

To solve an N channel problem Fano (1970) defines N^2 elements of the $U_{i\alpha}$ matrix and N, μ_α phase shifts. Whereas, Cooke and Cromer (1985) construct a symmetric matrix with only N(N+1)/2 total elements from the $U_{i\alpha}$ matrix and from the μ_α phase shifts. Therefore, we rewrite the MQDT equation (2.29b) in a way that eliminates $U_{i\alpha}$ and μ_α elements in a favour of symmetric matrix. Hence, following Cooke and Cromer, Biag and Bhatti (1994), the straightforward calculation gives a relation for the phase shifted MQDT reaction matrix as:

$$[R + \varepsilon]a = 0, \qquad 2.31$$

where R is the interaction matrix having zero diagonal elements and the off-diagonal elements $R_{i\,j}$ describe the interaction between the ith and jih channels. ε is the diagonal matrix having components for the bound channels as:

$$\varepsilon_i = \tan[\,\pi\,(\nu_i + \mu_i\,)], \qquad 2.32$$

where μ_i is the quantum defect and ν_i is the effective quantum number of the ith bound channel with respect to the ith ionization limit. The a_i is the column vector given by:

$$a_i = A_i \cos[\pi\,(\nu_i + \mu_i\,)] \qquad 2.33$$

where A_i being the amplitude of the ith collisional channel. For a non-trivial solution of the equation (2.31), we have:

$$\det|\ R + \varepsilon\ | = 0 \qquad 2.34$$

Quantum defect graphical representation

The two most important attributes of a discrete Rydberg spectrum, characterised by quantum number J and parity, are the number of interacting channels N and different series limits M. The number of series limits is less than or equal to the number of interacting channels i.e. $M \leq N$. The number M of series limits involved in the multichannel interaction is simply the number of distinct states of the core occurring in the channels which interact to produce the observed spectrum.

Each observed energy level has as many effective principal quantum numbers as there are number of series limits M. The effective quantum numbers ν_i for a level of energy E are determined from the following equation:

$$E = I_i - (R_y / \nu_i^2), \qquad 2.35$$

where I_i is the ith ionization limit and R_y is the Rydberg constant. These i number of equations give (i -1) independent relations of the following form :

$$I_i - (R_y / \nu_i^2) \;= I_j - (R_y / \nu_j^2). \qquad i \neq j \qquad 2.36$$

These i -I set of equations determines a "line" in the i dimensional space of the ν_i . This line plays an important role in determining the theoretical positions of the bound states.

The ν_i are nonintegers (except for hydrogen) and its noninteger part contains the information about the mutual interactions among Rydberg series due to electron-electron effects. Therefore, it is the characteristic feature of MQDT that the effective quantum

numbers are considered modulo 1. The quantum defect μ is given by the fractional part of $-\nu$ i.e.,

$\mu = -\nu \bmod 1$.

Considering the two channel interaction, as in the case of rare gases for J = 0 with odd parity, the effective quantum numbers ν_1 and ν_2 for an energy level E_n are extracted with respect to the two ionization limits I_1 and I_2 by using the following relation:

$$E_n = I_1 - (R/\nu_1^2) = I_2 - (R/\nu_2^2). \qquad 2.37$$

The MQDT compatibility equation (2.36) for two channel model is :

$$\begin{vmatrix} \tan \pi(\nu_1 + \mu_1) & R_{12} \\ R_{21} & \tan \pi(\nu_2 + \mu_2) \end{vmatrix} = 0 \qquad 2.38$$

Where μ_1 and μ_2 are the quantum defect and R_{12} is the interaction parameter between the two channels. The quantum defect plot is generated as shown in figure (2.5) by plotting the ν_1 (mod. 1) verses ν_2 (mod. 1).

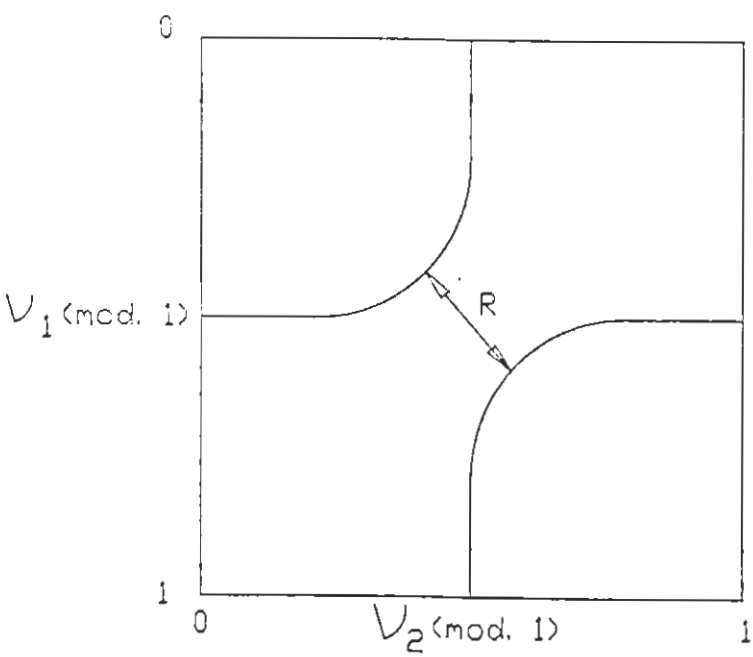

Figure (2.5) Lu - Fano plot. Fractional part of the effective quantum numbers ν_1 (mod. 1) with respect to the first ionization limit are plotted versus fractional part of the effective quantum numbers ν_2 (mod. 1) with respect to the second ionization limit.

CHAPTER 3

EXPERIMENTAL DETAILS

3.1 Laser System

The laser system which we have used for the experiment as an excitation source is an excimer pump dye laser system (Lambda Physik, Germany). The excimer laser (XeCl), model EMG 101 MSC, filled with a gas mixture (xenon = 80 mbar, HCl = 100 mbar, neon = 2420 mbar and total gas pressure = 2600mbar) gave the laser radiation at 308 nm with an output energy of about 60 - 80 mJ. The repetition rate of the laser can be varied from 1 to 50 Hz. This laser was used to pump the dye laser model Fl 2002 EC. The dye laser is comprised of oscillator and amplifier stages. The pulse dye laser can be tuned from 332 nm to 970 nm using different dyes. The band width of the dye laser is 0.2 cm^{-1} (6GHZ) at 500nm.This can be reduced by using interacavity etalon up to 0.04cm^{-1} (1.2GHZ). The pulse width of the dye laser is about 12nsec.The tuning element of the dye laser, a 1200 lines/mm grating, is coupled with a stepper motor. The scanning is controlled by a scanning unit model FL 583. The scanning range, scan step and scan speed can be conveniently adjusted. The minimum scan step, which is the wavelength change per motor step is 0.0042 nm / grating order.

3.2 Discharge Cell

We have designed a discharge cell (Fig. 3.1) for the laser optogalvanic studies of the rare gases. It consists of a glass tube 120 mm long and 30 mm in diameter with quartz windows on each side. Two cylindrical nickel electrodes of 10 mm diameter with an interelectrode separation of 25 mm are inserted in the cell through tungsten rods of 1 mm diameter. For an incoming laser the hollow electrodes provide an uninterrupted passage through the cell. The cell is connected to the evacuation and gas fill system. The

evacuation system consists of rotary and diffusion pumps. The cell is cleaned with a rare gas discharge before filling it up with the rare gas for the spectroscopic studies.

3.3 Data Acquisition System

In pulsed mode, a boxcar integrator can be used for noise reduction and signal amplification to improve the quality of the signal of interest. Stanford Research System's boxcar model SR 250 has been used for such purpose. The SR 250 consists, basically, of a gate generator, a fast gated integrator and an averaging circuitry. The gate generator can be triggered from an internal clock from 1 to 10 kHz or from an external triggering source. The gate's position with respect to the trigger can be varied from a few nanoseconds to 100 milliseconds. The fast gated integrator integrates the input signal during the time the gate is open. The output from the integrator is then normalized by the gate width to provide a voltage which is proportional to the average of the input signal during the sampling gate. The signal is amplified by the sensitivity setting of the instrument which is from 1V/1V to 1V/5mV - volts out / volts in. The 'signal output' and the 'gate' are fed to a dual channel oscilloscope, triggered from the boxcar 'busy output'. The sampling gate, with the boxcar delay controls, can be positioned with respect to the signal. The boxcar samples the gated portion of the signal and averages it at the selected value.

3.4 Experimental Set Up

Fig 3.1 shows the experimental set up. The excimer pump dye laser at 7 HZ rep. rate is focused into the discharge cell by an 80 mm focal length lens. The DC power supply (Hewlett-Packard 6448B) is connected to the cell through a ballast resistor to produce a glow discharge. The OG signal is monitored via coupling capacitor. We simultaneously irradiated with the same laser beam a commercial hollow cathode lamp for the wavelength calibration of the experimental data. The voltage signals from the hollow cathode lamp and the discharge cell were processed by two boxcar averagers (SR 250). The gate's positions / widths of both the boxcar averagers were optimized for the best signal to noise ratio. Using an oscilloscope, the gate positions were so adjusted to sample only the peak of the voltage signals. We recorded the signals on a dual channel chart

recorder (Philips PM 8262, Xt). The signals obtained from the hollow cathode lamp, using the assignments of Striganov and Sventitskii (1968), served as the frequency markers for the measurement of the spectrum obtained from the discharge cell. The linearity of the dye laser scan between two wavelengths (generated by the hollow cathode lamp) is checked. The accuracy of the measuring wavelength is ~ 0.3 cm^{-1}. The linearity lies within this error.

The experimental set up described above is similar for our work on krypton and xenon. We optimized the discharge parameters before recording the spectra. The discharge cell was evacuated to mbar and then filled with rare gas (krypton and xenon). The cell was connected with the DC power supply through a ballast resistor of 60kΩ and OG voltage signal was monitored through a coupling capacitor of 0.1μF. For a good signal to noise ratio, DC discharge was operated at about 240 volts at a krypton pressure of about 0.6 mbar. The Ryodamine-B and Ryodamine- 101 dyes at an energy of about ~ 5 mJ were used to scan the spectral region from 654nm to 592nm for the measurement of two photon spectra of krypton. For the wavelength calibration of the experimental data, a commercial neon hollow cathode lamp was simultaneously irradiated with the same laser beam.

For the study of xenon Rydberg states, the discharge cell was operated at about 250 volts at a pressure of 0.4 mbar. The DCM dye was used to scan the 680nm to 635nm spectral region. A commercially available hollow cathode lamp of argon was simultaneously irradiated with the same laser. The ballast resistor and the coupling capacitor were the same as used for krypton. It may be mentioned here that xenon poses special problems for stable discharge. The wall loading effect of xenon is quite pronounced. A freshly filled cell gives a good optogalvanic signal but the signal detriotes quickly. If the cell is cleaned with a xenon discharge (for about half an hour) before filling, stable and quite operation for longer periods can be achieved.

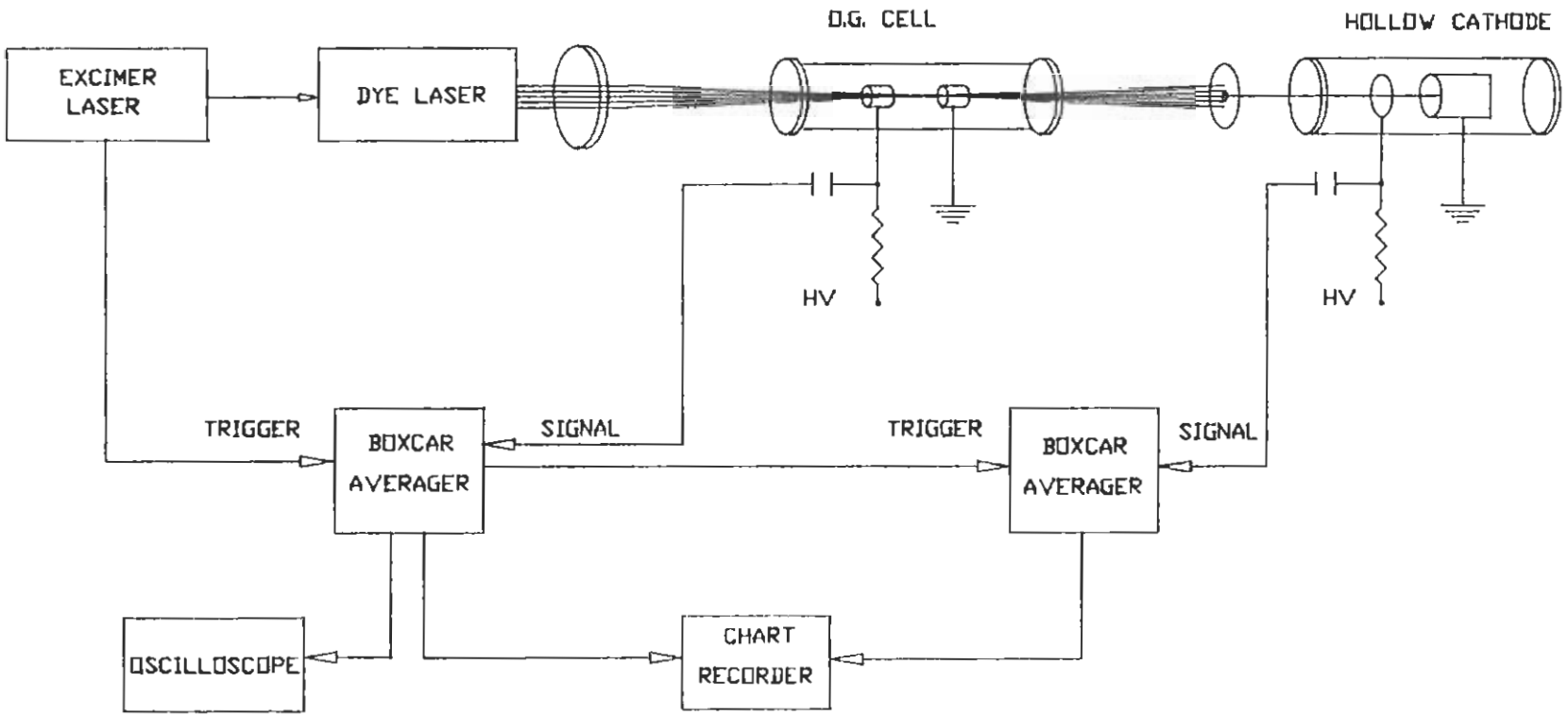

Figure (3.1) Schematic diagram of the experimental set up.

CHAPTER 4

Two Photon Laser Optogalvanic Spectroscopic Studies of Krypton

4.1 Introduction

The odd parity high Rydberg series of krypton have been extensively studied by Yoshino and Tanaka (1979), Delsart et al (1981a,b), and Yoon and Glab (1994). The J = 1 Rydberg series (bound and autoionized) were studied by Yoshino and Tanaka (1979) in absorption using a 6.65-m spectrograph. Strong series interactions were reported and analyzed through the multichannel quantum defect theory. Delsart et al. (1981a,b) excited the $4p^5nd$ J = 1, 2, 3 and $4p^5ns$ J = 1, 2 series via two step multiphoton excitation using two different techniques namely an atomic beam and optogalvanic detection in a D.C. discharge. Simultaneously Aymar et al (1981) analyzed the available data on odd parity states for J = 0, 1, 2, 3 by means of MQDT and theoretically simulated the odd parity spectrum of krypton. Yoon and Glab (1994) re-examined the previous work of the odd parity series of krypton and reported the high n Rydberg series using step wise two photon excitation from the $4p^55s[3/2]_2$ level. Yoon and Glab (1994) also determined the ionization potentials (I.P) from each of the observed odd parity Rydberg series with much higher accuracy, and quoted an average value of the I.P. as 112914.50 (0.014) cm^{-1}. For the even parity level the detailed work was presented by Bounakhla et al (1993) using the laser optogalvanic method and investigated the spectra originating from the levels belonging to 4p4d and 4p5s configurations.

In the present work we have implied the two photon laser optogalvanic technique for the study of odd parity Rydberg series of krypton. The observed series are excited from the $4p^55s[3/2]_2$ and $4p^55s'[1/2]_0$ metastable levels. The observed spectra may be interpreted with the aid of the partial term diagram shown in figure (4.1). A total of ten odd parity Rydberg series $4p^5nd[1/2]_{0,1}$, $4p^5nd[3/2]_2$, $4p^5nd[5/2]_{2,3}$, $4p^5nd[7/2]_{3,4}$, $4p^5ns[3/2]_2$, $4p^5ns'[1/2]_0$ and unresolved $4p^5nd'[3/2]_2$ (or $4p^5nd'[5/2]_2$) Rydberg series have been observed. The $4p^5nd[1/2]_0$, $4p^5nd[7/2]_4$, $4p^5nd'[3/2]_2$ or $4p^5nd'[5/2]_2$ and

$4p^5ns'[1/2]_0$ series for high n values are reported for the first time. We have also tried to fill the existing gap between the energy values of Moore (1952) and that of Delsart et al (1981a,b). The MQDT analysis for J = 0, 2 and 3 has been performed. Another interesting feature of our work is the observation of an even parity Rydberg series $4p^5np[1/2]_1$ (two photon parity forbidden transitions).

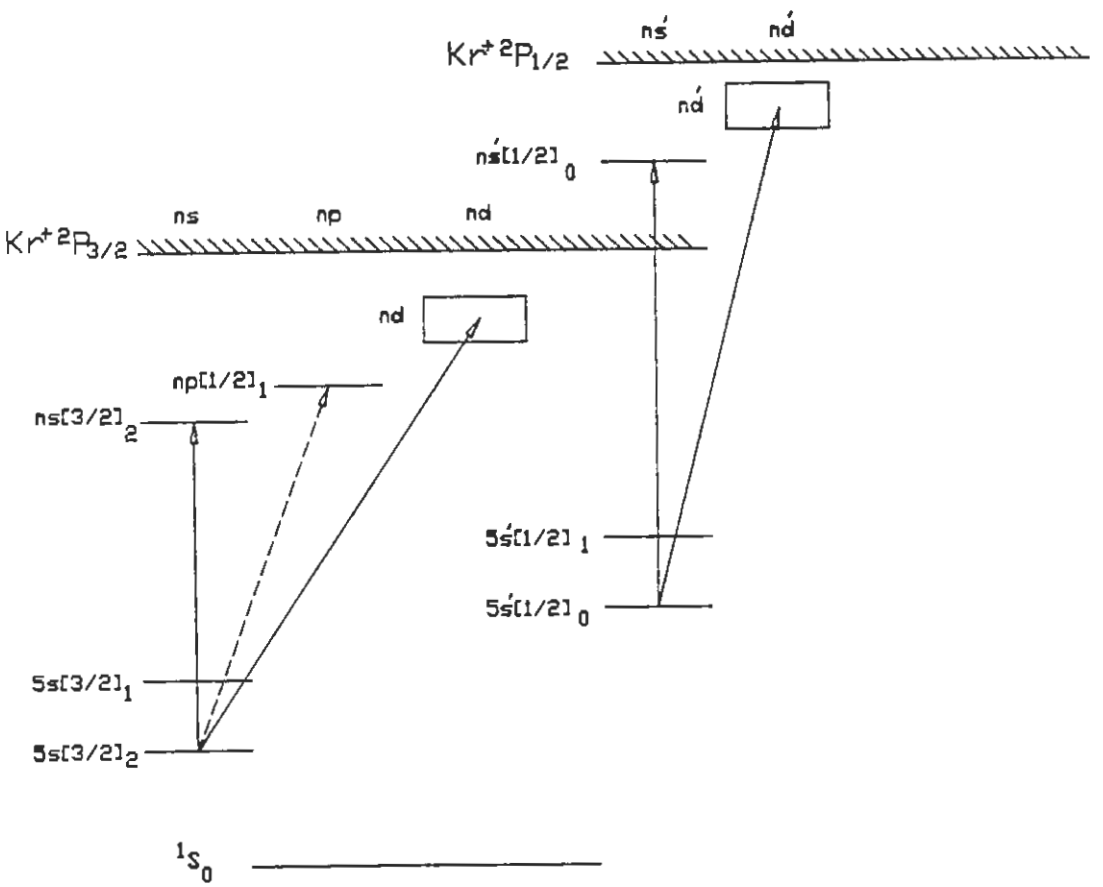

Figure (4.1) Partial term diagram for krypton. Transitions of the type observed in the present experiment are indicated by arrows.

4.2 RESULTS AND DISCUSSION

4.2.1 Two photon spectra

Figure (4.2) shows a part of the two photon laser optogalvanic Rydberg spectra of krypton observed in the region 16507cm^{-1} to 16342 cm^{-1}. The upper trace is the single photon laser optogalvanic (LOG) spectrum of the neon hollow cathode lamp used for the calibration of the observed data. The energy values of the lines are taken from the table of the spectral lines of the neutral and ionized atoms (Striganov and Sventitskii 1968). On the top of the figure a few Rydberg series are marked. The spectrum exhibits typical inert gas features. The Rydberg series are clearly seen to be converging to the two ionization limits $4p^5(^2p_{3/2})$ and $4p^5(^2p_{1/2})$. The intensities of the series converging to the first ionization limit $4p^5(^2P_{3/2})$ are much stronger than the series converging to the limit $4p^5(^2p_{1/2})$.

The inert gas spectrum (except helium) can be most conveniently designated in a Jℓ coupling scheme. For krypton the ground state is $4p^6(^1S_0)$. The first excited manifold has four levels namely $4p^5 5s[3/2]_{2,1}$ and $4p^5 5s'[1/2]_{0,1}$. The $4p^5 5s[3/2]_2$ and $4p^5 5s'[1/2]_0$ levels are metastable, whereas the $4p^5 5s[3/2]_1$ level is semi-metastable. In a discharge there is a considerable population of these levels. The observed two photon spectrum is a result of laser induced excitations from these levels. We have not observed any transitions originating from the $4p^5 5s'[1/2]_1$ level due to its strong coupling to the ground state (Yoshino and Tanaka 1979). The parity conservation dictates two photon excitation to ns and nd levels only. With the two photon selection rule $\Delta J = 0, \pm 1, \pm 2$, we can access ten possible odd parity Rydberg series converging to the ionization limit $4p^5(^2p_{3/2})$. These are $4p^5 nd[1/2]_{0,1}$, $4p^5 nd[3/2]_{1,2}$, $4p^5 nd[5/2]_{2,3}$, $4p^5 nd[7/2]_{3,4}$, and $4p^5 ns[3/2]_{1,2}$. We have observed all these series. Similarly, out of six possible $4p^5 nd'[3/2]_{1,2}$, $4p^5 nd'[5/2]_{2,3}$ and $4p^5 ns'[1/2]_{0,1}$ Rydberg series converging to the $4p^5(^2p_{1/2})$ ionization limit, only $4p^5 ns'[1/2]_0$ and the unresolved $4p^5 nd'[3/2]_2$ or $4p^5 nd'[5/2]_2$ series are observed.

The absolute term values in wave-numbers for the observed Rydberg levels are calculated by the relation

$$T_n = A + 2E_n$$

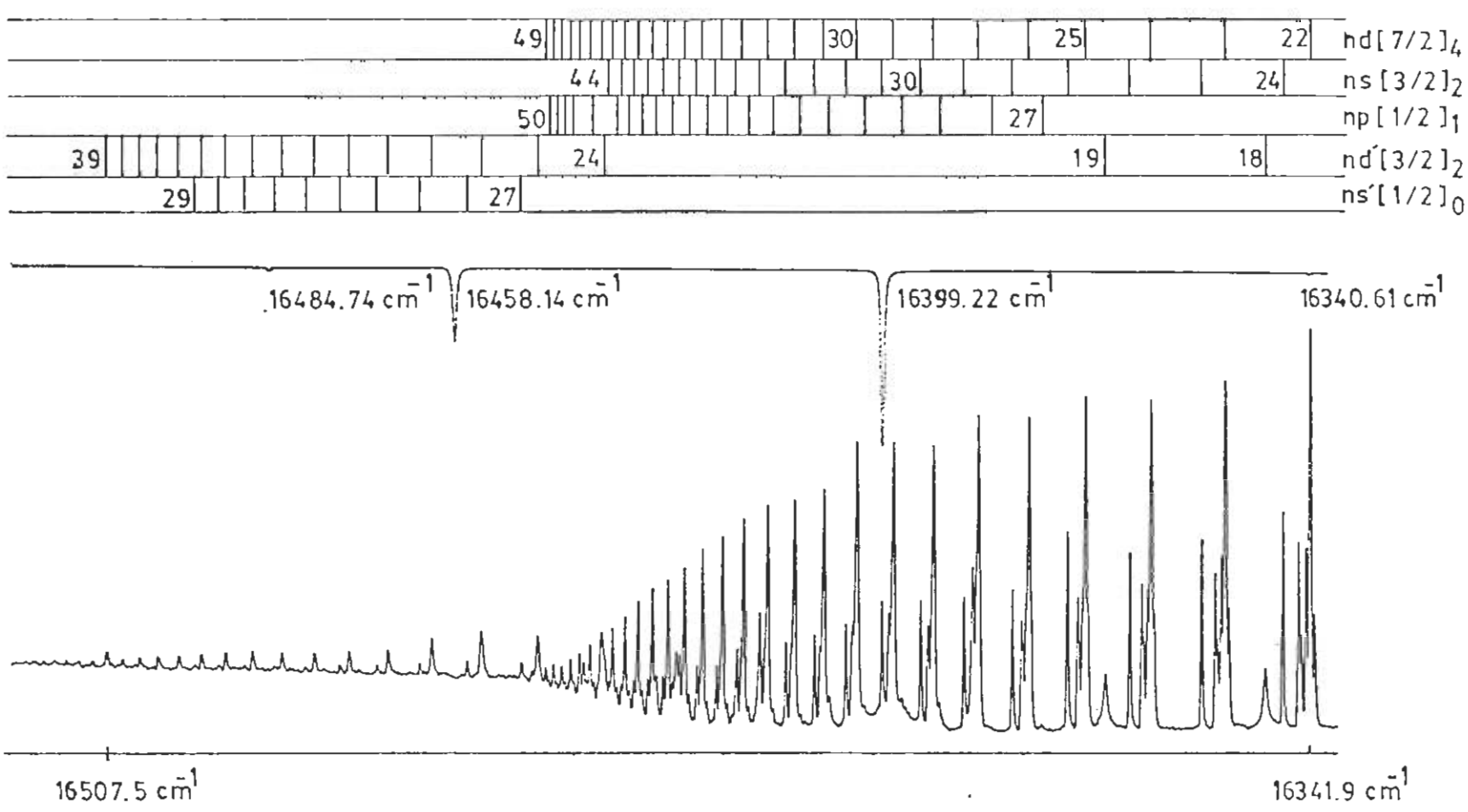

Figure (4.2) Two photon laser optogalvanic spectrum of krypton. Upper trace is the hallow cathode laser optogalvanic spectrum of neon for calibration. Assignments of a few Rydberg series are indicated at the top.

where E_n is the observed transition energy and A is the energy of the corresponding metastable level.

The identification of the upper levels is made using the selection rules for the optical transitions and extrapolations of the data from the lower n values. The energies of the $4p^5 5s$ configuration levels together with the ionization potentials used in the calculations are listed in Table (4.1). The measured energy values of the observed Rydberg series and their assignments are listed in the Tables (4.2, 4.3 and 4.4).

Table (4.2) shows the absolute energy values of the odd parity $4p^5 ns$ and $4p^5 nd$ Rydberg series excited from the $4p^5 5s[3/2]_2$ level and terminating to the $4p^5(^2P_{3/2})$ limit. At lower n the observed energy values are in good agreement with the previous data (Delsart a,b 1981). At higher n values the observed energies are systematically lower (~ 0.3 cm^{-1}) than the values quoted in the literature (Delsart 1981, Yoon and Glab 1994). This may be attributed to the quadratic Stark effect due to electric field in the discharge cell.

The $4p^5 nd[1/2]_0$ series is the weakest and $4p^5 nd[7/2]_4$ is the strongest one. The intensity of the series $4p^5 nd[5/2]_2$ decreases slowly with the increase of n as compared to other series. The relative intensities (with respect to $4p^5 nd[7/2]_4$) of the observed series $4p^5 nd[1/2]_0$, $4p^5 nd[1/2]_1$, $4p^5 nd[3/2]_2$, $4p^5 nd[7/2]_3$, $4p^5 nd[5/2]_2$, $4p^5 nd[5/2]_3$ and $4p^5(n+2)s[3/2]_2$ are about (0.07), (0.25), (0.5), (0.38), (0.15), (0.38) and (0.5) respectively around n = 21.

The Rydberg series $4p^5 nd[3/2]_1$ and $4p^5 ns[3/2]_1$ have not been observed from the $4p^5 5s[3/2]_2$ metastable level. However, laser excitations from the $4p^5 5s]3/2]_1$ level to a few members of the $nd[3/2]_1$ and $ns[3/2]_1$ Rydberg series have been observed at higher sensitivities. Figure (4.3) shows a portion (15480 cm^{-1} - 15560 cm^{-1}) of the spectrum recorded at five times more sensitivity (trace a) as compared to other data (trace b). The transitions marked as 1 and 2 are the single photon transitions, namely $4p^5 5p[5/2]_3 \rightarrow 4p^5 6d[7/2]_4$ and $4p^5 5p[5/2]_2 \rightarrow 4p^5 6d[3/2]_2$. The transitions marked 3 - 7 are the two photon transitions from the $4p^5 5s[3/2]_1$ level to $4p^5 12d[3/2]_2$, $4p^5 12d[5/2]_{2,3}$, $4p^5 12d[3/2]_1$ and $4p^5 14s[3/2]_1$ levels respectively. The signal from these transitions is almost 30 times weaker than the weakest series $4p^5 nd[1/2]_0$ observed from the $4p^5 5s[3/2]_2$ level. We have

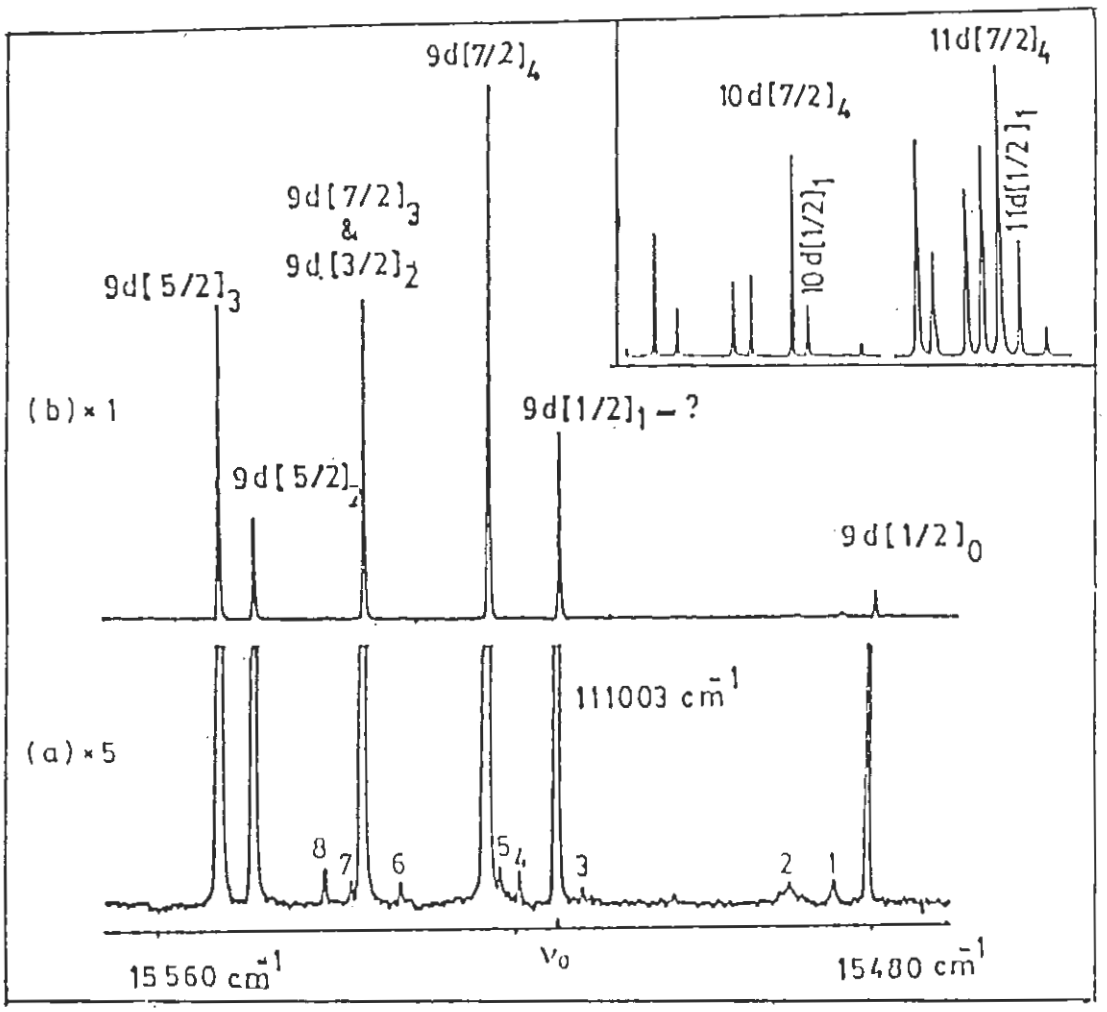

Figure(4.3) . Laser optogalvanic spectrum of krypton in the region 15480 - 15560 cm^{-1}. The optogalvanic signal of lower portion (a) was recorded on a scale five times more sensitive than the upper trace (b). The inset shows the resolved structure for the 10d and 11d multiplets. The transitions marked as 1 and 2 are the one photon transitions namely $4p^5 5p[5/2]_3 \rightarrow 4p^5 6d[7/2]_4$ and $4p^5 5p[5/2]_2 \rightarrow 4p^5 6d[3/2]_2$ and The numbers 3-7 represents the two photon transitions from the $4p^5 5s[3/2]_1$ to $4p^5 12d[3/2]_2$, $4p^5 12d[5/2]_{2,3}$, $4p^5 12d[3/2]_1$ and $4p^5 14s[3/2]_1$ levels respectively. The number 8 represent the two photon transition $4p^5 5s[3/2]_2 \rightarrow 4p^5 7s'[1/2]_0$.

not scanned the entire spectrum at higher sensitivities, only $4p^5nd[3/2]_{1,2}$, $4p^5nd[5/2]_{2,3}$, $4p^5nd[7/2]_3$ and $4p^5(n+2)s[3/2]_1$ for n = 11, 12 and 13 were recorded.

The Rydberg series terminating to the second ionization potential $4p^5(^2p_{1/2})$ are excited from the $4p^55s'[1/2]_0$ level, which are $4p^5ns'[1/2]_0$ series and an unresolved $4p^5nd'[3/2]_2$ or $4p^5nd'[5/2]_2$ series. The energies of these Rydberg series are listed in Table (4.3). The $4p^57s'[1/2]_0$ and $4p^58s'[1/2]_0$ levels of the $4p^5ns'[1/2]_0$ series are excited from the $4p^55s[3/2]_2$ level. The unresolved auto-ionized $4p^5nd'[3/2]_2$ or $4p^5nd[5/2]_2$ lines are broader and much stronger than respective $4p^5ns'[1/2]_0$ lines. The width of the autoionized transitions decreases with the increase of principal quantum number n. The observed full width at half maximum (FWHM) of the $4p^5nd'[3/2]_2$ (or $4p^5nd'[5/2]_2$) Rydberg series at lower n values is about 11 cm^{-1} (n = 8) and at higher n values FWHM ~ 1.0 cm^{-1} (n = 27). Similarly FWHM of the $4p^5ns'[1/2]_0$ Rydberg series is about 5 cm^{-1} and 0.5 cm^{-1} at n = 10 and 28 respectively. The transition marked 8 in figure(4.3) at absolute energy value 111055 cm^{-1} is the two photon transition from $4p^55s[3/2]_2$ to $4p^57s'[1/2]_0$ level. This is in excellent agreement with the value 111065 ±10 cm^{-1} predicted by Aymar et al (1981) based on the MQDT.

The assignment of the level at absolute energy value 111003 cm^{-1} has attracted much attention in the literature. This level was assigned as $4p^5\ 7s'[1/2]_1$ in the NBS Tables (Moore 1952). Kaufman and Humphrey (1969) reassigned it as $4p^59d[1/2]_1$. Yoshino and Tanaka (1979) agreed with the NBS Table (Moore 1952), on the basis of the MQDT analysis. However, Aymar et al (1981) assigned the line at the energy value 111072 cm^{-1} as $4p^5\ 7s'[1/2]_1$ and the line at 111003 cm^{-1} as $4p^5\ 9d[1/2]_1$. Their assignment was based on the calculation of the percentage admixture coefficients. The calculation showed 32% $d[3/2]_1$, 31% $d[1/2]_1$, and 27% $s'[1/2]_1$ coefficients for the line at 111003 cm^{-1} and 60% $s'[1/2]_1$, 15% $d[3/2]_1$ and 17% $d[1/2]_1$ coefficients at 111072 cm^{-1}. The relative intensity of the line marked ν_0 in figure (4.3) at absolute energy 111003 cm^{-1} with respect to the $4p^59d[7/2]_4$ level is almost the same as the relative intensity of other members of $4p^5nd[1/2]_1$ Rydberg series with respect to the corresponding member of the $nd[7/2]_4$ series. This is clear from the $4p^5nd$ multiplet structure given in the inset (Fig. 4.3) for n = 10 and 11. In view of the above analysis, the assignment of the line at 111003 cm^{-1} as

$9d[1/2]_1$ seems more appropriate and is in accord with the assignments given by Kaufman and Humphrey (1969) and Aymer (1981).

4.2.2 MQDT Analysis

Strong irregularity was observed in the $4p^5nd[3/2]_2$ Rydberg series. At n = 9 it blends with the $9d[7/2]_3$ level and subsequently it appears on the higher energy side of the $4p^5nd[7/2]_4$ Rydberg series. At n = 15 it again merges with the $4p^5nd[7/2]_4$ series before reappearing at n = 19 on the lower energy side of the $4p^5nd[7/2]_4$ series. This is a typical series interaction behaviour which is analyzed using multi-channel quantum defect theory.

The MQDT analysis for J = 0, 1, 2 and 3 was performed by Aymer et al (1981). For J = 0 they used the energy values for $4 \leq n \leq 11$ from NBS Table (Moore 1952). In the present work we have extended the $4p^5nd[1/2]_0$ series up to n = 22 and also observed the $4p^57s'[1/2]_0$ level experimentally. We have performed the MQDT analysis for J = 0 based on this new and extended data for which there are only two possible interacting channels, namely $4p^5nd[1/2]_0$ and $4p^5ns'[1/2]_0$. Although the orbital angular quantum number of the excited levels are different their K and J quantum numbers are same. The effective quantum numbers ν_1 and ν_2 for an energy level E_n are calculated with respect to the two ionization limits $I_{3/2}$ and $I_{1/2}$ by using the following relation:

$$E_n = I_{3/2} - R_y/(\nu_1)^2 = I_{1/2} - R_y/(\nu_2)^2,$$

where R_y is the mass corrected Rydberg constant (109736.6 cm^{-1}) for krypton. We identify channel 1 as $4p^5nd[1/2]_0$ and channel 2 as $4p^5ns'[1/2]_0$. The MQDT compatibility equation for the two channel model is (Giusti - Suzor and Fano 1984, Cooke and Cromer 1985, Baig and Bhatti 1994):

$$\begin{vmatrix} \tan \pi(\nu_1 + \mu_1) & R_{12} \\ R_{21} & \tan \pi(\nu_2 + \mu_2) \end{vmatrix} = 0,$$

where μ_1 and μ_2 are quantum defects with respect to the ionization limits at 112914.6 cm^{-1} and 118284.6 cm^{-1} respectively. R_{12} is the interaction parameter. In figure (4.4 a) the Lu- Fano plot for J = 0 is shown. The open circles indicate new data and the solid circles show data points taken from the literature. The solid curves passing through the data points represent the MQDT parameters. The perturber $4p^57s'[1/2]_0$ (shown as ✯) also lies on the theoretical curve which was not observed previously but predicted from

the MQDT analysis by Aymer et al (1981). The MQDT parameters are $\mu_1 = 0.47$, $\mu_2 = 0.115$ and $R_{12} = 0.140$.

For J = 3 levels, the MQDT compatibility equation for the three channel model is:

$$\begin{vmatrix} \tan \pi(\nu_1 + \mu_1) & R_{12} & R_{13} \\ R_{21} & \tan \pi(\nu_2 + \mu_2) & R_{23} \\ R_{31} & R_{32} & \tan \pi(\nu_3 + \mu_3) \end{vmatrix} = 0.$$

To extract the MQDT parameters, we identify channel 1 as $4p^5nd\ [5/2]_3$, channel 2 as $4p^5nd[7/2]_3$ both having the ionization limit at 112914.6 cm^{-1} and channel 3 as $4p^5nd'[5/2]_3$ with ionization limit at 118284.6 cm^{-1}. Since the series limits are well established, the fractional part of the effective quantum numbers $\nu_{3/2}$(mod.1) with respect to the first ionization limit are plotted against the fractional part of the effective quantum numbers $\nu_{1/2}$(mod.1) with respect to the second ionization limit (Fig.4.4 b). The theoretical solid curves, passing through the data points yield the MQDT parameters as $\mu_1 = 0.293$, $\mu_2 = 0.340$, $\mu_3 = 0.298$, $R_{12} = 0.100$, $R_{13} = 0.155$, $R_{23} = 0.150$. The magnitude of the interaction parameter R_{13} is nearly the same as R_{23}. Whereas, the interaction parameter R_{12} which shows the interaction between the series belonging to the same ionization limit (nd × nd) is 1.5 times smaller than the series interaction among the channels belonging to the two different limits (nd × nd').

For the J = 2 Rydberg series, we have used a five channel MQDT model. We identify channel 1 as $4p^5nd[3/2]_2$, channel 2 as $4p^5nd[5/2]_2$, channel 3 as $4p^5ns[3/2]_2$, channel 4 as $4p^5nd'[5/2]_2$ and channel 5 as $4p^5nd'[3/2]_2$. The first three channels converge to the $4p^5(^2P_{3/2})$ ionization limit and the last two channels to the $4p^5(^2P_{1/2})$ limit. The Lu-Fano plot for the bound levels is shown in the figure(4.4 c). The MQDT parameters are tabulated as follows:

$\mu_1 = 0.369$	$\mu_2 = 0.305$	$\mu_3 = 0.111$	$\mu_4 = 0.321$	$\mu_5 = 0.340$
$R_{12} = 0.050$	$R_{13} = 0.160$	$R_{14} = 0.310$	$R_{15} = 0.130$	$R_{23} = 0.001$
$R_{24} = 0.001$	$R_{25} = 0.250$	$R_{34} = 0.040$	$R_{35} = 0.110$	$R_{45} = 0.001$

The strongest interaction is between $4p^5nd[3/2]_2$ and $4p^5nd'[5/2]_2$ which is almost double than the interaction between $4p^5nd[3/2]_2$ and $4p^5ns[3/2]_2$. Another strong interaction is between $4p^5nd[5/2]_2$ and $4p^5nd'[3/2]_2$ which is almost 1.6 times than the interaction

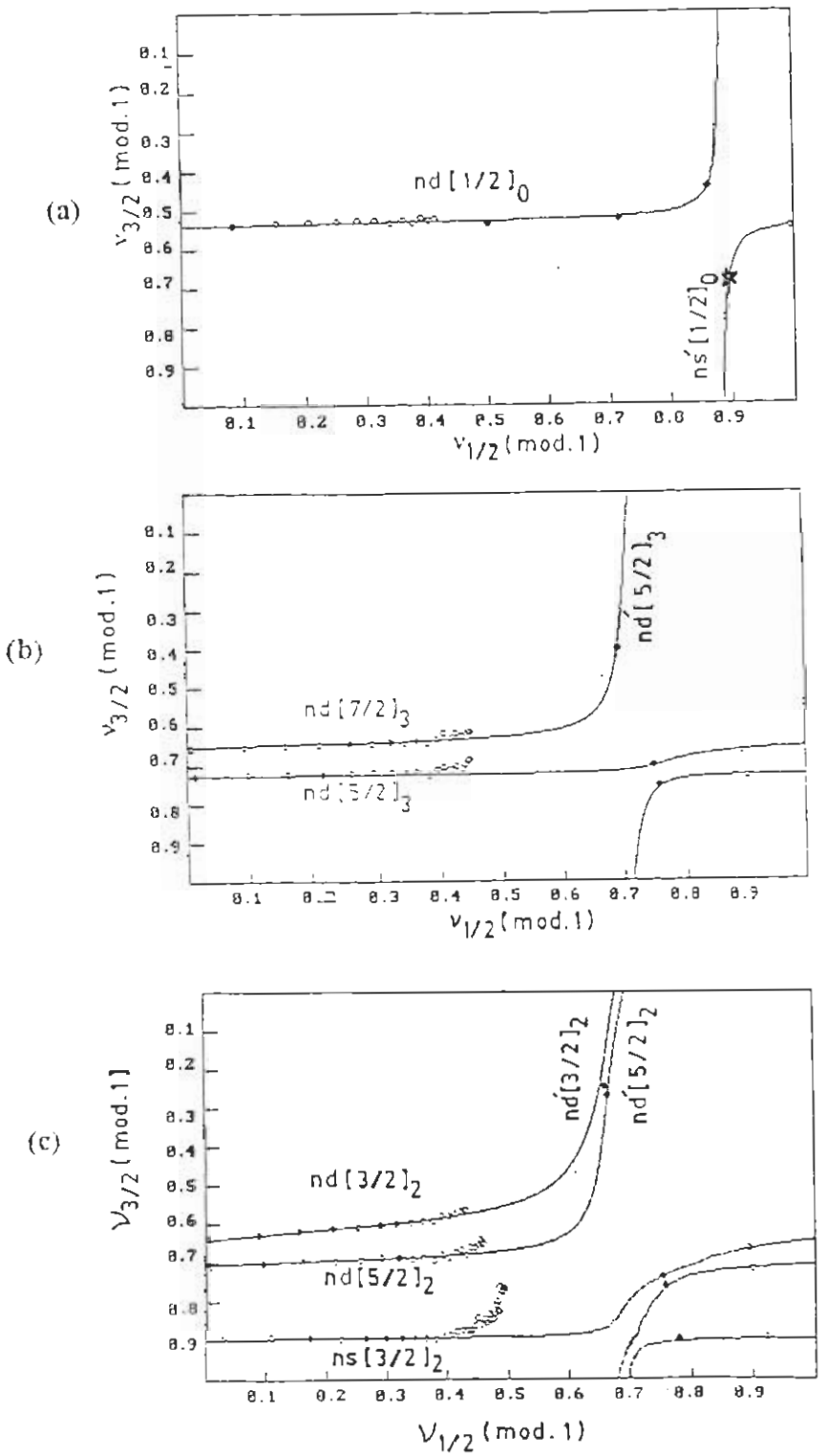

Figure (4.4) Lu - Fano plot for the bound levels of krypton. Fractional part of the effective quantum numbers $\nu_{3/2}$ (mod. 1) are plotted versus $\nu_{1/2}$ (mod. 1) with different J values. (a) J = 0, (b) J = 3 and (c) J = 2.

between $4p^5nd[3/2]_2$ and $4p^5ns[3/2]_2$. In comparison the interaction between the series nd' × nd' converging to the $4p^5(^2P_{1/2})$ ionization limit is very small (R_{45} = 0.001) relative to the interaction (R_{12}= 0.050) between the series nd × nd converging to the $4p^5(^2P_{3/2})$ ionization limit.

4.2.3 Two Photon Parity Forbidden Transitions

Besides the odd parity two photon Rydberg series already discussed, another feature of the spectra is the periodic appearance of a line at the longer wavelength side of $4p^5nd[1/2]_1$ series. These lines can be grouped in to a Rydberg series. The energies of this series is tabulated in Table(4.4). This series starts from n = 26 and remains observable to the first ionization limit. The relative intensity of these transitions increases with the increase of the principle quantum number n (see Fig 4.2) If we consider the laser excitation to be taking place from the $4p^55s[3/2]_2$ level then the measured two photon energy values are in a good agreement with the $4p^5np[1/2]_1$ series reported by Audouard et al (1990). This implies a two photon laser excitation from an odd parity $4p^55s[3/2]_2$ level to even parity $4p^5np[1/2]_1$ levels. These transitions are two photon parity forbidden. If we focus the laser in the region of the discharge where the electric field is high then these transitions appear at lower n values and shift towards the longer wavelength side. In view of the above observation the fact that these two photon parity forbidden transitions seem to be due to the electric field.

Ito et al (1993) also observed one photon parity forbidden transition in krypton in the presence of electric field. They observed $4p^5np[1/2]_0$, $4p^5np[1/2]_1$, $4p^5np[3/2]_{1,2}$ and $4p^5np[5/2]_2$ series at lower n values. Their energy values shift towards the longer wavelength side with the increase of the electric field. According to their calculations, the $4p^5np[1/2]_1$ and $4p^5np[3/2]_2$ series are due to Stark mixing of the $4p^5nd[1/2]_1$ series. We have not observed the $4p^5np[3/2]_2$ transitions. This may be due to the reason that it lies closer in energy to the strongest series $4p^5nd[7/2]_4$ and the observation is beyond our spectral resolution. The observed two photon energy values are smaller than the values reported by Audouards et. al. 1990. This shift in the energy values may be due to the presence of the electric field in the discharge.

4.3 CONCLUSION

In conclusion we have studied the odd parity Rydberg series of krypton using single colour two photon laser optogalvanic spectroscopy. A total of eleven Rydberg series excited from the $4p^5 5s[3/2]_2$ and $4p^5 5s'[1/2]_0$ metastable levels have been observed. The MQDT analysis of the interacting Rydberg series for the J = 0, 2 and 3 has been attempted. We have also reported the observation of two photon parity forbidden Rydberg series. This seems to be appearing due to Stark mixing of levels. The electric field is also causing a shift in the energy levels, especially at higher n values.

It is suggested that the following studies can be carried out by extending the present work.

- The spectra can be made more rich by reducing the band width of the laser.
- The transition probabilities for two photon transitions can be measured.
- Multichannel quantum defect theory analysis of the autoionzed levels.
- The electric field measurements at various positions in the discharge cell can be made by measuring the line intensity ratio of the forbidden to allowed transitions or by the energy level shifts. These analysis require that observed transitions must be out of the saturation effects.

TABLE - 4.1 Ionization potentials and absolute energy values (cm^{-1}) of levels corresponding to the $4p^5 5s$ configuration of krypton.

$IP(^2P_{3/2})$	112914.6[a]
$IP(^2P_{1/2})$	118284.6[a]
$5s[3/2]_2$	79971.73[b]
$5s[3/2]_1$	80916.7575[b]
$5s'[1/2]_0$	85191.6075[b]
$5s'[1/2]_1$	85846.6945[b]

[a] Yoshino and Tanaka (1979)

[b] Bounakhla et al (1993)

TABLE -4.2 Absolute energy values (cm^{-1}) of the Rydberg series of krypton excited from the $4p^5 5s[3/2]_2$ metastable level and converging to the $4p^5(^2P_{3/2})$ ionization limit.

n	$nd[1/2]_0$	$nd[1/2]_1$	$nd[3/2]_2$	$nd[7/2]_4$	$nd[7/2]_3$	$nd[5/2]_2$	$nd[5/2]_3$	$(n+2)ns[3/$
9	110933.1	111003.0	a	111018.8	111046.7	111071.8	111078.8	111154.5
10	111412.3	111428.3	111445.0	111433.0	111450.3	111467.2	111474.0	111527.5
11	111708.7	111718.4	111731.3	111725.6	111736.9	111748.5	111754.0	111793.2
12	111925.5	111931.9	111941.7	111938.8	111946.9	111956.0	111960.3	111990.0
13	112089.4	112093.8	112101.2	112099.5	112105.5	112112.8	112116.3	112139.4
14	112215.8	112219.0	112224.7	112224.0	112228.2	112233.7	112236.5	112254.7
15	112315.1	112317.4	b	112321.4	112325.0	112329.1	112331.5	112346.1
16	112394.7	112396.4	b	112399.9	112402.7	112406.1	112408.0	112420.0
17	112459.8	112460.9	b	112463.7	112466.2	112469.0	112470.6	112480.3
18	112512.9	112513.9	b	112516.2	112518.2	112520.6	112522.0	112530.1
19	112557.7	112558.5	112560.1	112560.5	112562.1	112564.1	112565.4	112572.1
20	112594.7	112595.4	112596.8	112597.1	112598.6	112600.2	112601.2	112607.1
21	112626.8	112627.1	112628.4	112628.6	112630.0	112631.5	112632.3	112637.2
22	112654.1	112654.4	112655.4	112655.7	112656.8	112657.9	112658.8	112662.9
23	112677.5	112677.8	112678.7	112679.0	112679.9	112680.9	112681.6	112685.3
24		112698.5	112699.1	112699.4	112700.2	112701.3	112701.8	112704.9
25		112716.3		112717.1	112718.0	112718.6	112719.2	112722.1
26		112732.1		112732.8	112733.5	112734.2	112734.5	112737.1
27				112746.4		112747.9		112750.3
28				112758.7		112760.0		112762.5
29				112770.0		112771.1		112773.1
30				112780.1				112782.8
31				112788.8				112791.3
32				112797.0				112799.3
33				112804.4				112806.5
34				112811.0				112812.8

35	112817.0	112818.6
36	112822.6	112824.0
37	112827.6	112829.1
38	112832.1	112833.4
39	112836.3	112837.7
40	112840.6	112841.6
41	112844.2	112845.14
42	112847.7	112848.6
43	c	
44	112853.8	
45	112856.6	
46	112859.1	
47	112861.6	
48	112863.8	
49	112865.9	

The transitions a, b and c are omitted due to their overlap with $9d[7/2]_3$, $nd[7/2]_4$ and 24d'[3/2] respectively.

TABLE -4.3 Absolute energy values (cm^{-1}) of the Rydberg series of krypton excited from the $4p^5 5s'[1/2]_0$ metastable level and converging to the $4p^5(^2P_{1/2})$ ionization limit.

n	$nd'[3/2]_2$, $nd'[5/2]_2$	$ns'[1/2]_0$
7		111055.0[a]
8	115793.0	113695.0[a]
9	116400.5	
10	116810.5	115975.5
11	117101.4	116524.5
12		116898.0
14	117596.8	117360.0
15	117694.2	117509.3
16	117772.0	
17	117835.0	117716.9
18	117887.5	117790.7
19	117931.2	
23	118049.8	
24	118070.6	
25	118087.8	
26	118103.3	
27	118117.0	118092.0
28	118129.3	118107.0
29	118140.2	118120.5
30	118150.1	118132.3
31	118159.0	118143.0
32	118167.3	118152.5
33	118174.5	118161.0
34	118181.0	118169.0
35	118187.0	118176.2
36	118192.8	118182.6
37	118197.8	
38	118202.1	
39	118206.6	

a- These Rydberg series members were excited from the $4p^5 5s[3/2]_2$ level.

TABLE -4.4 Absolute energy values of the $np[1/2]_1$ Rydberg series of krypton excited from the $4p^5 5s[3/2]_2$ metastable level and converging to the $4p^5(^2P_{3/2})$ ionization limit.

n	$np\,[1/2]_1$
27	112729.3
28	112743.3
29	112756.1
30	112767.5
31	112777.6
32	112786.8
33	112795.0
34	112802.7
35	112909.4
36	112815.6
37	112821.3
38	112826.1
39	112831.3
40	112835.2
41	112839.4
42	112843.0
43	112846.3
44	
45	112852.5
46	
47	112858.1
48	112861.1
49	112863.1
50	112865.2

CHAPTER 5

Two photon Laser Optogalvanic Spectroscopic Studies of Xenon

5.1 Introduction

The detailed previous studies of the odd parity high Rydberg series of xenon have been reported by (Labastie et al 1982, Yoshino and Freeman 1985, Wang and Knight 1986). Labastie et al (1982) observed the $5p^5ns$ and $5p^5nd$ Rydberg series for J = 0, 1, 2, 3 and 4 excited from $5p^56p$ levels using one photon laser optogalvanic detection in xenon r.f. discharge. The J = 1 Rydberg series were studied by Yoshino and Freeman (1985) in the absorption spectrum of xenon with a 6.65-m vacuum spectrograph and Bonin et al (1985) using XUV laser excitation spectroscopy. Wang and Knight (1986) observed the $5p^5ns'$ and $5p^5nd'$ Rydberg series using two photon laser spectroscopy from the $6s[3/2]_2$ metastable level via various $5p^56p'$ (J = 1,2) intermediate levels. The even parity Rydberg series have been studied by Stebbings et al (1975), Grandin and Husson (1981), and knight and Wang (1985 and 1986).

The present work involves laser optogalvanic studies of xenon Rydberg atom using two photon excitation. To the best of our knowledge the D. C discharge optogalvanic studies are reported for the first time. We have observed eight odd parity (two photon allowed) Rydberg series and one even parity (two photon forbidden) Rydberg series excited from the $5p^56s[3/2]_2$ metastable level. The observed spectra can be interpreted with the aid of the partial term diagram shown in figure (5.1). The observed series are $5p^5nd[1/2]_{0,1}$, $5p^5nd[3/2]_2$, $5p^5nd[7/2]_{3,4}$, $5p^5nd[5/2]_{2,3}$, $5p^5ns[3/2]_2$ and $5p^5np[5/2]_2$. The $5p^5nd[1/2]_0$, $5p^5nd[7/2]_4$, and $5p^5ns[3/2]_2$ series up to higher n values are reported for the first time. The MQDT analysis for J = 0, 2 and 3 has been performed.

Besides two photon Rydberg series we have also observed a number of one photon transitions series excited from configuration in the reported spectral region. Some of them can be grouped into two $5p^5$ nf Rydberg series.

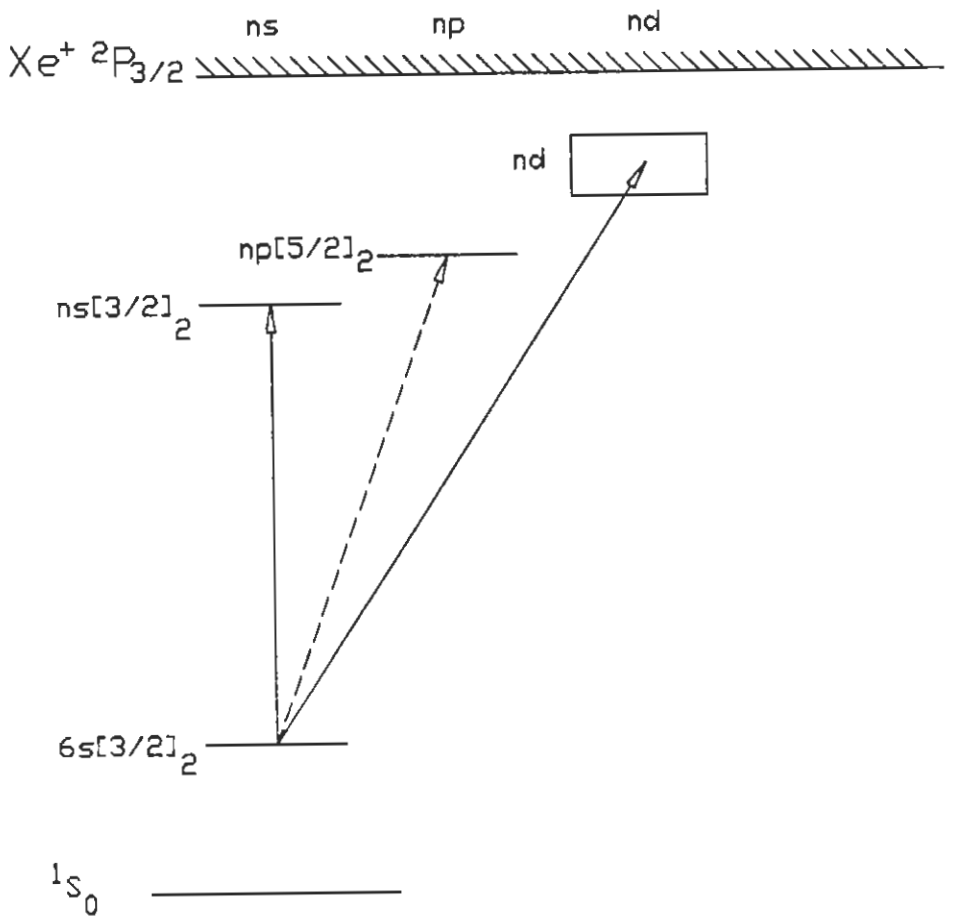

Figure (5.1) Partial term diagram for xenon. The two photon transitions observed in the present experiment are indicated by arrows.

5.2 RESULTS AND DISCUSSION

5.2.1 Two photon spectra

Figure (5.2) shows a part of the two photon single colour laser optogalvanic Rydberg spectra of xenon observed in the region 658nm - 650nm. The upper trace is the single photon LOG spectrum of the argon hollow cathode lamp used for the calibration of the observed data. On the top of the figure a few series are marked. The Rydberg series are clearly seen converging to the first ionization limit $5p^5(^2P_{3/2})$.

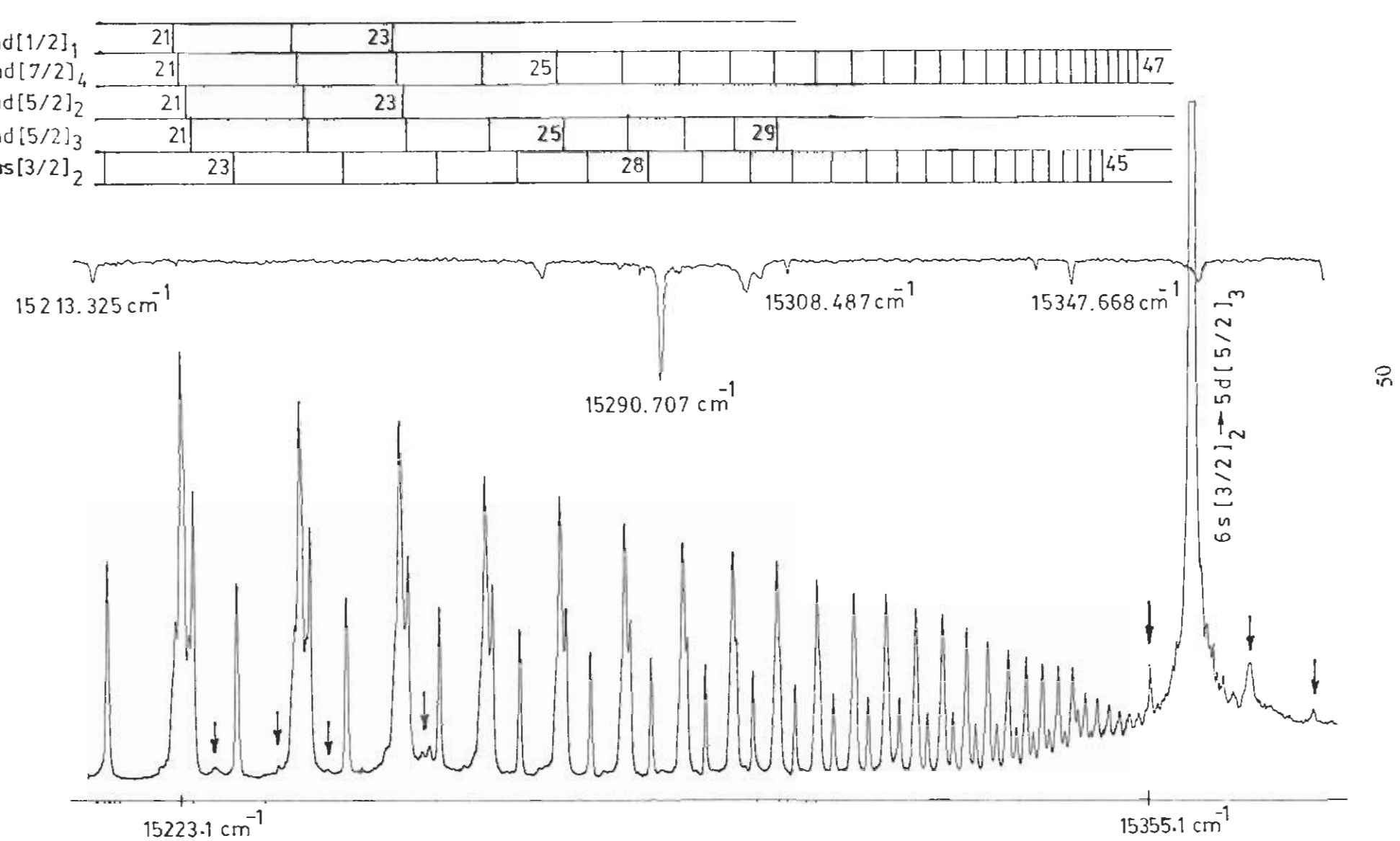

Figure (5.2) Two photon laser optogalvanic spectrum of xenon. Upper trace is the hallow cathode laser optogalvanic spectrum of argon for calibration. Assignments of a few Rydberg series are indicated at the top. ↓ indicates the si

The laser excitation wavelengths are converted into wave-numbers by using the formula (Radzig and Smirnov 1985). The energy levels position of the observed transitions are converted to absolute value with respect to the ground state by adding the energy (expressed in wave-number) of the corresponding lower metastable level. Therefore, the absolute term values in wave-numbers for the observed Rydberg levels are calculated by using the relation

$$T_n = A + 2E_n$$

where E_n is the energy of the observed transition and A is the energy in wave-number of the corresponding metastable level. The energy values for the lower n excited states of xenon have been reported by Humphreys and Paul (1970) and Moore (1958). The assignment of an observed transition needs identification of both the upper and the lower levels. In the discharge only a few metastable are excited and have sufficient population to permit laser excitation and hence optogalvanic detection. In xenon the first excited levels above the ground state ($^1S_0$) are four levels of the $5p^5 6s$ configuration. These levels are listed in table (5.1). The $5p^5 6s[3/2]_2$ and $5p^5 6s'[1/2]_0$ levels are metastable. In the discharge these levels have considerable population. Therefore, we expect one of these two levels to act as the lower level in the laser induced excitation. The identification of upper levels depend upon the selection rules for the optical transitions and on the extrapolation of the data from the lower n values.

In the present work all observed two photon Rydberg series terminating to the first ionization limit $5p^5(^2P_{3/2})$ are excited from the $5p^5 6s[3/2]_2$ level. Transitions excited from the $5p^5 6s[3/2]_2$ level and terminating to the second ionization limit $5p^5\,^2P_{1/2}$ were not observed because these do not lie in the laser scan spectral region. In krypton, argon and neon studies, two photon laser induced excitations from the $5p^5 6s'[1/2]_0$ metastable level have been reported (Ahmed et al 1997, Piracha et al 1997, 1996). In xenon we did not observe any transition from the level $5p^5 6s'[1/2]_0$ up to the laser scanning region 635 nm. A Possible reason for this peculiar behaviour in xenon is the breakdown of jl coupling as reported by Knight and Wang (1985) while observing $\Delta l = 3$ transitions from this level. According to their explanation, configuration interaction strongly admixes the $5p^5 5d[1/2]_0$

level with the $5p^5 6s'[1/2]_0$ level. The metastable level is 66% $5p^5 6s'[1/2]_0$ and 34% $5p^5 5d[1/2]_0$.

Eight out of ten possible $5p^5ns$ and $5p^5nd$ odd parity Rydberg series have been observed. The observed series, designated in $j\ell$ coupling scheme, are $5p^5ns[3/2]_2$, $5p^5nd[1/2]_0$, $5p^5nd[1/2]_1$, $5p^5nd[3/2]_2$, $5p^5nd[5/2]_2$, $5p^5nd[5/2]_3$, $5p^5nd[7/2]_3$ and $5p^5nd[7/2]_4$.Table (5.2) shows the absolute measured energy values of these Rydberg series excited from the $5p^5 6s[3/2]_2$ level. The measured energy values are in good agreement with the energies reported in the literature at lower n values (Labastie et al 1982). However there is a systematic shift at higher n values. At n = 47 the shift in the $5p^5nd[7/2]_4$ series is observed to be ~-0.6cm^{-1} as compared to the calculated values using the quantum defect 2.2794 reported by (Labastie et al 1982). This shift may be attributed to the electric field in the discharge. It was also observed that the width of the two photon transitions (FWHM ~ 0.4 cm^{-1}) is independent of principal quantum number n.

The relative intensities of the observed series $5p^5nd[1/2]_0$, $5p^5nd[1/2]_1$, $5p^5nd[7/2]_4$, $5p^5nd[7/2]_3$, $5p^5nd[5/2]_2$, $5p^5nd[5/2]_3$ and $5p^5(n+2)s[3/2]_2$ are about (0.22), (0.36), (1), (0.72), (0.36), (0.75), and (0.4) respectively at n = 18 and 19. The $5p^5nd[1/2]_0$ series is the weakest and $5p^5nd[7/2]_4$ is the strongest. The $5p^5nd[1/2]_0$ series was observed up to n = 21. Further observation was prevented due to the weakness of the series. The $5p^5nd[1/2]_1$, $5p^5nd[3/2]_2$, $5p^5nd[7/2]_3$, $5p^5nd[5/2]_2$, and $5p^5nd[5/2]_3$ series are observed up to n = 23, 17, 21, 22 and 29 respectively. Further observation of these series was not possible due to their closeness and overlap with the $5p^5nd[7/2]_4$ series. The strongest series $5p^5nd[7/2]_4$ and the series $5p^5ns[3/2]_2$ have been observed up to n = 47 and 44 respectively. Further observation was not possible due to poor S/N ratio.

5.2.2 MQDT Analysis

The MQDT analysis for J = 0, 1, 2 and 3 was performed by Lu (1971) using energy values for $n \leq 14$. In the present work we have extended the $5p^5nd[1/2]_0$, $5p^5nd[3/2]_2$, $5p^5nd[5/2]_2$, $5p^5ns[3/2]_2$, $5p^5nd[7/2]_3$ and $5p^5nd[5/2]_3$ series up to n = 21, 17, 22, 44, 21 and 29 respectively. We have performed the MQDT analysis for J = 0, 3 and 2 of bound states. For J = 0 there are only two possible interacting channels, namely

$5p^5nd[1/2]_0$ and $5p^5ns'[1/2]_0$. Although the orbital quantum number of the excited states are different but their K and J quantum numbers are same. The effective quantum numbers ν_1 and ν_2 for an energy level E_n are calculated with respect to the two ionization limits $I_{3/2}$ and $I_{1/2}$ using the relation:

$$E_n = I_{3/2} - R_y/(\nu_1)^2 = I_{1/2} - R_y/(\nu_2)^2$$

Where R_y is the mass corrected Rydberg constant (109736.86 cm^{-1}) for xenon. We identify channel 1 as $5p^5nd[1/2]_0$ and channel 2 as $5p^5ns'[1/2]_0$. The MQDT compatibility equation for two channel model is (Giusti - Suzor and Fano 1984, Cooke and Cromer 1985, Baig and Bhatti 1994):

$$\begin{vmatrix} \tan \pi(\nu_1 + \mu_1) & R_{12} \\ R_{21} & \tan \pi(\nu_2 + \mu_2) \end{vmatrix} = 0,$$

where μ_1 and μ_2 are quantum defects with respect to the ionization limits at 97834.26 cm^{-1} and 108370.8 cm^{-1} respectively. R_{12} is the interaction parameter. In figure (5.3a) Lu- Fano plot for J = 0 bound levels is shown. The open circles are the present work data points and solid circles show the data points taken from the literature. The solid curve passing through the data points gives the MQDT parameters, which are $\mu_1 = 0.545$, $\mu_2 = 0.050$ and $R_{12} = 0.110$.

For J = 3 bound levels, the MQDT compatibility equation for three channels is:

$$\begin{vmatrix} \tan \pi(\nu_1 + \mu_1) & R_{12} & R_{13} \\ R_{21} & \tan \pi(\nu_2 + \mu_2) & R_{23} \\ R_{31} & R_{32} & \tan \pi(\nu_3 + \mu_3) \end{vmatrix} = 0.$$

To extract the MQDT parameters, we identify channel 1 as $5p^5nd[5/2]_3$, channel 2 as $5p^5nd[7/2]_3$ both having the ionization limit at 97834.26 cm^{-1}, and channel 3 as $5p^5nd'[5/2]_3$ with ionization limit 1083740.8 cm^{-1}. Since the series limits are well established, the fractional part of the effective quantum numbers with respect to the first ionization limit $\nu_{3/2}$(mod. 1) are plotted against the effective quantum numbers with respect to the second ionization limit $\nu_{1/2}$ (mod. 1) as shown in Fig.(5.3b). The theoretical curves passing through the data points yield the MQDT parameters as $\mu_1 = 0.430$, $\mu_2 =$

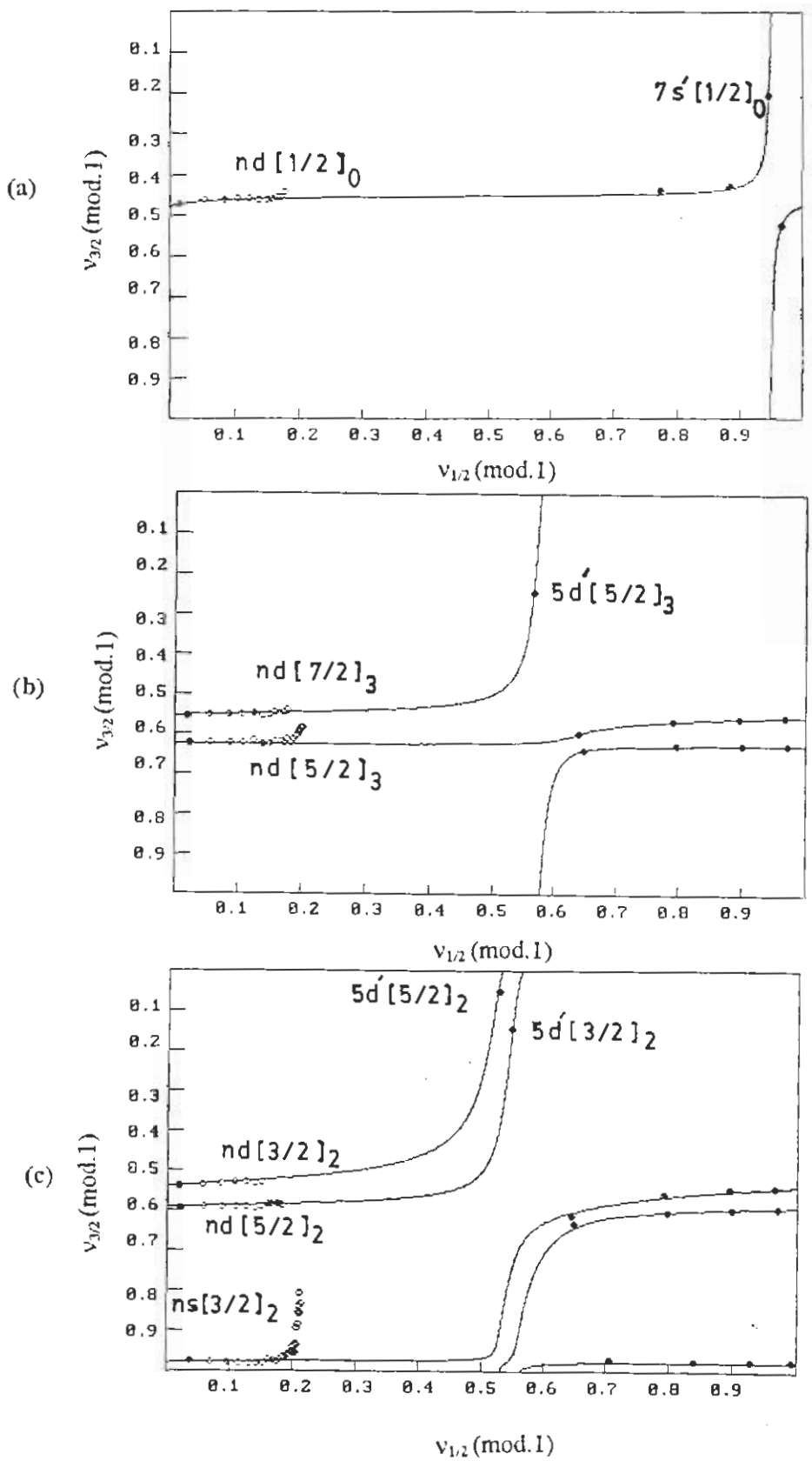

Figure (5.3) Lu - Fano plot for the bound levels of xenon. Fractional part of the effective quantum numbers $\nu_{3/2}$ (mod. 1) are plotted versus $\nu_{1/2}$ (mod. 1) with different J values. (a) J = 0, (b) J = 3 and (c) J = 2.

0.390, μ_3 = 0.425, R_{12} = 0.100, R_{13} = 0.140 and R_{23} = 0.150. The magnitude of the interaction parameter R_{13} is nearly same as R_{23}. Whereas, the interaction parameter R_{12} which gives the interaction between the series converging to the same ionization limit (nd × nd) is about 1.5 times smaller than the series interaction among the channels terminating at two different ionization limits (nd × nd').

For J = 2 bound levels we have used five channels MQDT model. We identify channel 1 as $5p^5nd[3/2]_2$, channel 2 as $5p^5nd[5/2]_2$, channel 3 as $5p^5ns[3/2]_2$, channel 4 as $5p^5nd'[3/2]_2$ and channel 5 as $5p^5nd'[5/2]_2$. The first three channels converge to the first ionization limit $5p^5(^2P_{3/2})$ and the last two channels to the second ionization limit $5p^5(^2P_{1/2})$. Lu - Fano plot for J = 2 bound levels is shown in the figure (5.3). The MQDT parameters are tabulated as follows:

$\mu_1 = 0.460$ $\mu_2 = 0.403$ $\mu_3 = 0.030$ $\mu_4 = 0.447$ $\mu_5 = 0.484$

$R_{12} = 0.050$ $R_{13} = 0.005$ $R_{14} = 0.250$ $R_{15} = 0.140$ $R_{23} = 0.250$

$R_{24} = 0.025$ $R_{25} = 0.240$ $R_{34} = 0.040$ $R_{35} = 0.070$ $R_{45} = 0.001$

Where μ_i and R_{ij} have their usual meaning.

The strongest interaction ($R_{14} = R_{23} \cong R_{25}$) is between $5p^5nd[3/2]_2$ and $5p^5nd'[3/2]_2$, $5p^5nd[5/2]_2$ and $5p^5ns[3/2]_2$, and $5p^5nd[5/2]_2$ and $5p^5nd'[5/2]_2$ although the series nd × ns belong to the same ionization limit $5p^5(^2P_{3/2})$. The interaction (R_{12} = 0.050) between $5p^5nd[3/2]_2$ and $5p^5nd[5/2]_2$ series is five times smaller than the interaction R_{14}(= 0.250). Whereas, the interaction between the series nd' × nd' converging to the second ionization limit $5p^5(^2P_{1/2})$ is very small (R_{45} = 0.001) as compared to the interaction (R_{12} = 0.050) between the series nd × nd converging to the first ionization limit $5p^5(^2P_{3/2})$.

5.2.3 Two Photon Parity Forbidden Transitions

Besides the odd parity two photon Rydberg series already discussed, another interesting feature consisting of periodic lines was observed at longer wavelength side of $5p^5nd[1/2]_0$ when the focused laser was moved about 10 mm away from the cathode. The lines could be grouped into a Rydberg series. If we consider the laser excitation to be taking place from $5p^56s[3/2]_2$ level then the measured two photon energy values are in good agreement with the $5p^5np[5/2]_2$ series reported by Blazewicz et al (1987). we have

observed this series from n = 16 up to n = 27. The energy values of this series are tabulated in Table (5.3).This series is due to two photon laser excitation from an odd parity $5p^5 6s[3/2]_2$ level to the even parity $5p^5 np[5/2]_2$ levels. These are two photon parity forbidden transitions. The appearance of this two photon parity forbidden Rydberg series is due to the Stark mixing of the levels as we moved the laser in discharge where the electric field is relatively high. Figure (5.4) shows a part of the two photon laser optogalvanic Rydberg spectra for the laser focused 10 mm away from the cathode. The assignments of the observed lines are marked at the top.

5.2.4 One Photon Transitions

In the reported spectral region we have also observed a number of one photon transitions. Some of them can be grouped into two Rydberg series. In the previous section, we have discussed the laser induced excitation from the levels belonging to $5p^5 6s$ configuration. Labastie et al (1982) remarked that discharge can populate the states of the $5p^5 6p$ configuration and reported the ns and nd Rydberg series excited from these levels. The levels belonging to the $5p^5 6d$ configuration have lifetime of the order of μsec (King and Latimer 1982) except those levels which are optically coupled with the ground state. Therefore, these states have steady state population in the discharge. King and Latmer (1982) have observed the $5p^5 np'$ and $5p^5 nf'$ transitions excited from the $5p^5 6d$ levels configuration. Grandin and Husson (1981) have observed a few $5p^5 nf'$ levels excited from the levels belonging to $5p^5$ 6d configuration. In the present studies we have observed that most of the single photon transitions are taking place from the levels belonging to $5p^5 5d$ configuration. These levels with their energy are list in table (5.1). The assignments of the upper levels depend on the selection rules i.e. the parity change during transition and that $\Delta J = 0, \pm 1$, ($0 \rightarrow 0$ excluded). The observed spectra can be interpreted with the aid of the partial term diagram shown in figure (5.5).

The energy values (expressed in wave number cm^{-1}) of the observed transitions with their assignment are tabulated in table (5.4). The transitions marked with * are available in the tables of spectral lines of neutral and ionized atoms (Striganov and

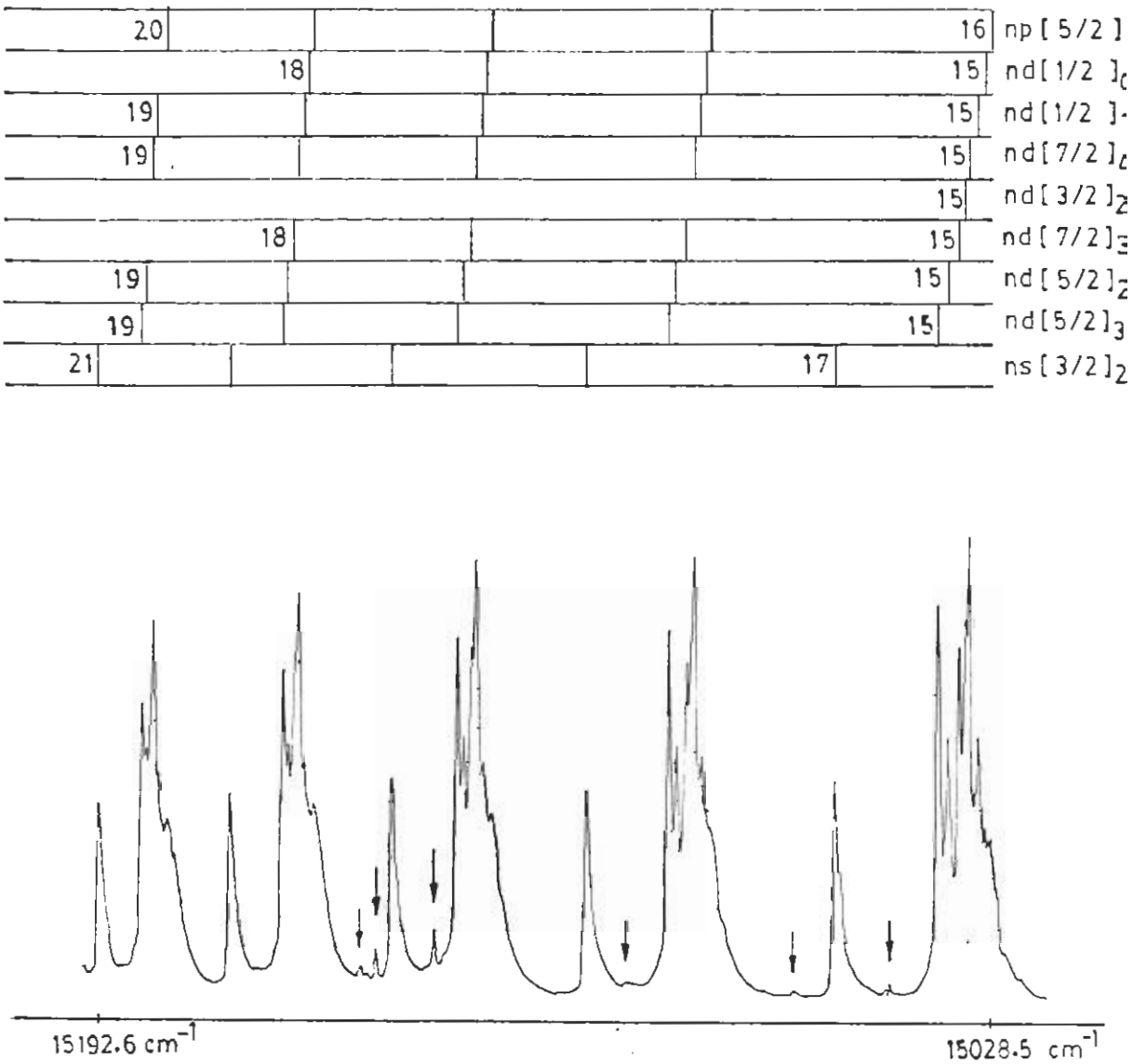

Figure (5.4) Two photon laser optogalvanic spectrum of xenon for the laser focusing about 10 mm away from the cathode. Assignments of the Rydberg series are indicated at the top. ↓ indicates the single photon transitions.

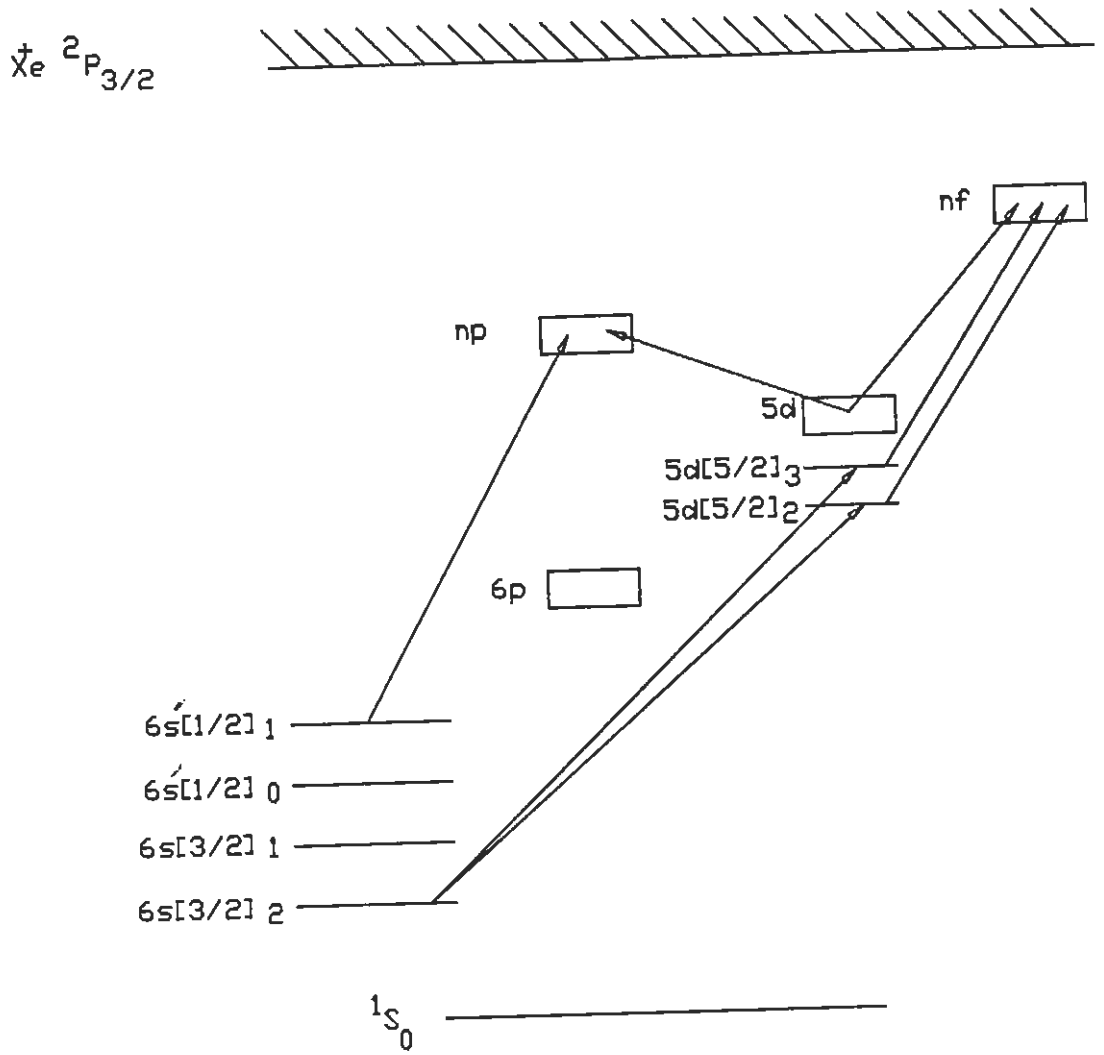

Figure (5.5) Partial term diagram for xenon. The single photon transitions observed in the present experiment are indicated by arrows.

Sventitskii 1968) and all other transitions are being reported for the first time. The measured values are in good agreement with data available in literature (Striganov and Sventitskii 1968 and Humphreys and Paul 1967). Besides these transitions we have also observed the $5p^5nf$ series excited from the level $5p^55d[5/2]_2$ and the level $5p^55d[5/2]_3$. The nf series, namely $5p^5nf[5/2]_{2,3}$ is excited from the level $5p^55d[5/2]_3$. This series was observed from n = 14 up to 31 and is listed in table (5.5). In addition a few other multiplet members were observed and are given in table (5.5). The other Rydberg series $5p^5nf$ consists of the multiplets $5p^5nf[5/2]_2$ and $5p^5nf[7/2]_3$ excited from the level $5p^55d[5/2]_2$. This was observed from n = 10 to 26. This series is listed in the table (5.6). All these multiplets of the $5p^5nf$ configuration are observed for the first time.

Almost all the observed one photon transitions and series are very weak as compared to the two photon Rydberg series except a few transitions namely $5p^5 5d[7/2]_3 \rightarrow 5p^5 nf[9/2]_4$, $5p^5 nf[7/2]_{3,4}$ and $5p^5 6s[3/2]_2 \rightarrow 5p^5 5d[5/2]_3$.

5.2.5 One Photon Parity Forbidden Transitions

The observed transitions at 15362.7 cm^{-1} (6507.50 A°) and 14857.9 cm^{-1} (6728.5A°) are due to the single photon laser excitation from the $5p^5 6s[3/2]_2$ level to the $5p^5 5d[5/2]_3$ and $5p^5 5d[5/2]_2$ levels, respectively. These transitions are single photon parity forbidden. The transition at 6507.50 A° is the strongest one in the entire observed spectra (see figure 5.2).

The appearance of the parity forbidden transitions cannot be attributed to the Stark mixing because the nearest $5p^5 6p$ state is 1807 cm^{-1} and 2311 cm^{-1} away from the levels $5p^5 5d[5/2]_2$ and $5p^5 5d[5/2]_3$ respectively. Knight et al (1982) have observed the Stark mixing of the states $5p^5 6d[1/2]_1$ with $5p^5 7p[3/2]_1$ in an electric field strength of about 4 kv/cm. Therefore, the stark mixing alone cannot explain the unusually strong transition observed in the present work as the discharge is running at a low potential of about 250 volts. However, the intense transition $5p^5 6s[3/2]_2 \rightarrow 5p^5 5d[5/2]_3$ can serve as a calibration line using LOG detection.

5.4 CONCLUSION

In conclusion we have studied the odd parity Rydberg series of xenon using single colour two photon laser optogalvanic spectroscopy. A total of nine Rydberg series excited from the $5p^5 6s[3/2]_2$ metastable level have been observed. The MQDT analysis of the interacting Rydberg series for the J = 0, 2 and 3 has been attempted. We have also reported the two photon parity forbidden series. Its appearance seems to be due to the Stark mixing of the levels. Besides these two photon measurements we have also observed a number of one photon transitions.

It is suggested that the following studies can be carried out by extending the present work.

- The transition cross sections for two photon transitions can be measured.

- The electric field measurements at various positions in the discharge cell can be made by measuring the line intensity ratio of the forbidden to allowed transitions or by the energy level shifts. These analysis require that the observed transitions must be out of the saturation effects.
- The autoionized Rydberg series can be excited from the $5p^5 6s[3/2]_2$ metastable level by using two photon single colour laser optogalvanic spectroscopy.

Table (5.1) Ionization potentials and absolute energy values (cm^{-1}) of lower levels involved in the laser excitation of xenon.

$IP(^2P_{3/2})$	97834.26[a]
$IP(^2P_{1/2})$	108370.8[b]
$5p^5 6s[3/2]_2$	67068.047[c]
$5p^5 6s[3/2]_1$	68045.663[c]
$5p^5 6s'[1/2]_0$	76197.292[c]
$5p^5 6s'[1/2]_1$	77185.560[c]
$5p^5 5d[1/2]_0$	79771.798[c]
$5p^5 5d[1/2]_1$	79987.16[c]
$5p^5 5d[7/2]_4$	80197.16[c]
$5p^5 5d[3/2]_2$	80323.28[c]
$5p^5 5d[7/2]_3$	80970.93[c]
$5p^5 5d[5/2]_2$	81926.04[c]
$5p^5 5d[5/2]_3$	82430.72[c]
$5p^5 5d[3/2]_1$	83890.47[c]

[a]Labastie et al (1982)

[b]Yoshino and Freeman (1985)

[c]Moore (1958)

Table (5.2) Absolute energy values (cm^{-1}) of the Rydberg series of xenon excited from the $5p^5 6s[3/2]_2$ metastable level and converging to the first ionization limit $5p^5(^2P_{3/2})$.

n	$nd[1/2]_0$	$nd[1/2]_1$	$nd[7/2]_4$	$nd[3/2]_2$	$nd[7/2]_3$	$nd[5/2]_2$	$nd[5/2]_3$	$ns[3/2]_2$
12	96608.6	96616.2	96622.7	96627.0	96631.5	96641.0	96648.9	
13	96831.7	96836.9	96842.1	96845.0	96848.8	96855.9	96861.7	
14	96998.9	97002.8	97007.2	97009.1	97012.0	97017.5	97022.1	96731.8
15	97127.35	97130.3	97134.0	97135.2	97137.5	97141.5	97145.2	96923.8
16	97228.9	97231.2	97234.1	97235.2	97237.2	97240.5	97243.3	97069.8
17	97309.0	97311.5	97313.9	97314.6	97316.1	97318.9	97320.2	97183.3
18	97375.1	97376.5	97378.6		97380.3	97382.5	97384.5	97272.9
19	97428.8	97429.8	97432.0		97433.2	97435.1	97436.5	97345.3
20	97474.1	97475.2	97476.9		97477.9	97479.5	97481	97404.0
21	97511.7	97512.9	97514.3		97515.0	97516.5	97517.6	97453.1
22		97545.2	97546.4			97548.3	97549.3	97494.8
23		97572.5	97573.7				97576.0	97529.4
24			97597.2				97599.2	97559.0
25			97617.8				97619.4	97584.6
26			97635.8				97637.2	97606.8
27			97651.6				97652.8	97626.1
28			97665.7				97666.6	97643.0
29			97678.1				97679.0	97657.9
30			97689.3					97670.4
31			97699.3					97683.2
32			97708.3					97693.7

33	97716.4	97703.4
34	97723.6	97711.8
35	97730.2	97719.6
36	97736.4	97726.4
37	97741.9	97732.8
38	97746.8	97738.5
39	97751.4	97744.1
40	97755.8	97748.9
41	97759.9	97753.4
42	97763.5	97757.7
43	97766.8	97761.4
44	97770.1	97765.1
45	97773.1	
46	97775.7	
47	97778.2	

Table(5.3) Absolute energy values (cm^{-1}) of the $5p^5np[5/2]_2$ Rydberg series of the xenon excited from the $5p^56s[3/2]_2$ metastable level.

n	$np[5/2]_2$
16	97125.1
17	97227.6
18	97307.7
19	97373.7
20	97427.2
21	97471.1
22	97508.8
23	97541.5
24	97569.0
25	97593.5
26	97614.1
27	97631.7

Table(5.4) One photon transitions.

Transitions	Energies(cm^{-1})	Transitions	Energies(cm^{-1})
$5p^5 6s[3/2]_2 \rightarrow 5p^5 5d[5/2]_2$	14857.9†	$5p^5 5d[7/2]_3 \rightarrow 5p^5 11p[5/2]_2$	14878.2
$5p6s[3/2]2 \rightarrow 5p5d[5/2]_3$	15362.7*†	$5p^5 5d[7/2]_3 \rightarrow 5p^5 11p[3/2]_2$	14909.1
$5p^5 6s'[1/2]_1 \rightarrow 5p^5 8p[1/2]_1$	14968.2*	$5p^5 5d[7/2]_3 \rightarrow 5p^5 8f[9/2]_4$	15130.5*
$5p^5 6s'[1/2]_1 \rightarrow 5p^5 8p[3/2]_1$	15148.0	$5p^5 5d[7/2]_3 \rightarrow 5p^5 8f[5/2]_3$	15135.9
$5p^5 6s'[1/2]_1 \rightarrow 5p^5 8p[3/2]_2$	15185.7*	$5p^5 5d[7/2]_3 \rightarrow 5p^5 8f[5/2]_2$	15137.1
$5p^5 6s'[1/2]_1 \rightarrow 5p^5 8p[1/2]_0$	15370.0*	$5p^5 5d[7/2]_3 \rightarrow 5p^5 8f[7/2]_{3,4}$	15140.9*
$5p^5 5d[1/2]_0 \rightarrow 5p^5 6f[3/2]_1$	14963.6*	$5p^5 5d[7/2]_3 \rightarrow 5p^5 9f[9/2]_4$	15495.8*
$5p^5 5d[1/2]_1 \rightarrow 6f[5/2]_2$	14773.2*	$5p^5 5d[7/2]_3 \rightarrow 5p^5 9f[7/2]_{3,4}$	15503.2*
$5p^5 5d[1/2]_1 \rightarrow 10p[3/2]_2$	15242.9	$5p^5 5d[3/2]_2 \rightarrow 5p^5 10p[5/2]_2$	14858.6*
$5p^5 5d[1/2]_1 \rightarrow 5p^5 7f[5/2]_2$	15590.7*	$5p^5 5d[3/2]_2 \rightarrow 5p^5 10p[5/2]_3$	14873.8
$5p^5 5d[1/2]_1 \rightarrow 5p^5 7f[3/2]_1$	15574.6*	$5p^5 5d[3/2]_2 \rightarrow 5p^5 10p[3/2]_2$	14907.0*
$5p^5 5d[1/2]_1 \rightarrow 5p^5 7f[3/2]_2$	15575.9*	$5p^5 5d[3/2]_2 \rightarrow 5p^5 11p[5/2]_2$	15526.3
$5p^5 5d[7/2]_4 \rightarrow 5p^5 10p[5/2]_3$	15000.0	$5p^5 5d[3/2]_2 \rightarrow 5p^5 11p[5/2]_3$	15535.7
$5p^5 5d[7/2]_4 \rightarrow 5p^5 11p[5/2]_3$	15661.7	$5p^5 5d[3/2]_2 \rightarrow 5p^5 7f[3/2]_1$	15238.0
$5p^5 5d[7/2]_4 \rightarrow 5p^5 7f[9/2]_{5,4}$	15370.4*		
$5p^5 5d[7/2]_4 \rightarrow 5p^5 7f[5/2]_3$	15379.1		
$5p^5 5d[7/2]_4 \rightarrow 5p^5 7p[7/2]_{3,4}$	15386.3*		

* Available in the literature (Striganov and Sventitskii 1968).

† single photon parity forbidden transitions.

Table(5.5) One photon transitions $5p^5 5d[5/2]_3 \rightarrow 5p^5 nf$

n	$nf[3/2]_2$	$nf[5/2]_{2,3}$	$nf[7/2]_{3,4}$
14	14840.4	14841.2	14842.1
15	14913.2	14914.0	14914.6
		unresolved	
16		14973.7	
17		15022.9	
18		15064.3	
19		15099.1	
20		15128.8	
21			
22		15176.1	
23		15195.4	
24			
25		15227.6	
26			
27			
28			
29		15272.0	
30			
31		15288.8	

Table(5.6) One photon transitions

$5p^5 5d[5/2]_2 \rightarrow 5p^5 nf$

n	$nf[5/2]_2$	$nf[7/2]_3$
10	14804.6	14806.5
11	14996.7	14998.1
12	15138.6	15139.2
13	15256.0	15256.9
14		
		UNRESOLVED
15		15419.2
16		15478.7
17		15527.7
18		15568.8
19		15603.5
20		15633.1
21		15658.9
22		15680.9
23		15700.5
24		15717.2
25		15732.0
26		15745.4

REFRENCES

Ahmed M, Zia M. A, Biag M. A and Suleman B. (1997)) J. Phys. B: At. Mol. Opt. Phys. vol. 30

Audorads E, Laporte P, Subtil J.L, Damany N and Pellarin M (1990) Phys. Rev. A **41,** 6032

Aymar M, Robaux O and Thomas C (1981) J.Phys. B: At. Mol. Phys. **14**, 4255

Baig M. A and Bhatti S. A (1994) Phys. Rev. A **50,** 2750

Baig M A and connerade J.P (1984) J.Phys.B: At. Mol. Phys. **17**, 1785

Barbieri B, Beverini N and Sasso A (1990) Rev. Mod. Phy. **62**, 603

Bebb H. B and Gold A (1966) Phys. Rev. **143**, 1

Berkowitz J (1979) " Photoabsorption, Photoionization and Photoelectron Spectroscopy " Academic Press

Beulter H (1935) Z. Phsik. **93,** 177

Blazewicz P. R, Stockdale J. A. D, Miller J. C, Efthimiopoulos T and Fotakis C (1987) Phys. Rev. A **35** 1092

Bloembergn and Levnson (1976) "High resolution Laser Spectroscopy", **13,** 315 (Springer- Verlag, New York)

Bounakhla M, Lemoigne J. P, Grandin J. P, Husson X, Kucal H and Aymar M (1993) J.Phys. B: At. Mol. Opt. Phys. **26**, 345

Bohr N (1913) Phil. Mag. **26,** 476.

Bokor J, Zavelovich J. Y and Rhodes C.K (1980) Phys. Rev. **A 21,** 1453

Bonin Keith D, McIlrath T. J and Yoshino K (1985) J. Opt. Soc. Am. **B2**, 1275

Bradley D. J, Ewart P, Nickolas V. J, and Shaw J. R. D (1973) J. Phys. B **6,** 1594

Bridges W. B (1978) J. Opt. Soc. Am. **68,** 352

Brune M, Raimond J. M, Goy P, Davidovitch L and Haroche S (1987) Phys. Rev. Lett. **59,** 1899

Camus P (1983) J. De Physik. Collqu. **C7,** 44

Camus P, Dieulin M and Morillon C (1979) J. Physique Lett. **40**, L513

Cederquist H and Mannervik (1982) J. Phys. B **15, L** 807

Connerade J. P, Lane A. M, and Baig M. A (1985) J. Phy. B **18**, 3507

Cooke W.E and Cromer C.L (1985) Phys. Rev. A **30**, 3057

Cooke W.E and Gallagher T. F (1978) Phys. Rev. A **19,** 1226

cowan R.D (1981) "The Theory of Atomic Structure and Spectra" University of california prees, Berkeley

Delsart C, Keller J-C and Thomas C (1981a) J.Phys. B: At. Mol. Phys. **14,** 4241

___ (1981b) J.Phys. B: At. Mol. Phys. **14,** 3355

Demtröder W (1981) " Laser Spectroscopy " Springer series in chemical physics 5, Springer-Verlag, Berlin

Dirac P. A. M (1958) "The Principle of Quantum Mechanics" 2nd edition Clarendon press Oxford

Dreze C, Demer Y, and Gagne J. M (1982) J. Opt. Soc. Am. **72**, 912

Edelstein S. A and Gallgher T. F (1978) Adv. At. Mol. Phys. **14** , 365

Ernst W. E, Softley T. P and Zare R. N (1988) Phys. Rev. A **37**, 4172

Fano U (1970) Phy. Rev. A **2**, 81

Fano U (1961) Phys. Rev. **124,** 1866

Flügge S (1956) ed. " Encyclopedia of Physics" Vol. XXII Electron-Emission Gas Discharges II Spriger-Verlag Berlin

Foot P.D and Mohler F. L (1925) Phys. Rev. **26,** 195

Glodsmith J. E. M and Lawler J. E (1981) Contemp. Phys. **22**, 235

Grandin J-P and Husson X (1981) J. Phys. B: At. Mol. Phys. **14**, 433

Green R. B, Keller R. A , Luther G. G, Schenck P. K and Travis J. C (1976) Appl. Phys. Lett. **29,** 727

Gallagher T. F (1994) "Rydberg Atoms" Cambridge University Press

Ganguly and Garscadden (1985a) Appl. Phys. Lett. **46,** 540

-(1985b) J. Appl. Phys. **57,** 4856

Guisti-Suzor A and Fano U (1984) J. Phys. B: **17,** 215

Harth K, Ganz J, Raab M, Lu K. T, Geiger J and Hotop H (1985) J. Phys. B: **18**, L825

Higgs C, Smith K. A, Dunning F. B and Stebbings R. F (1981) J. Chem. Phys. **75,** 745

Hippler M and Pfab J (1993) Optics Comm. **97**, 347

Humphreys C. J and Paul E. Jr (1970) J. Opt. Soc. Am. **60**, 1302

Hurst G. S and Panyne M. G (1988) " Principles and Applications of Resonance Ionisation Spectroscopy " Adam Hilger, Bristol and Philadelphia

Ito K, Masuda H, Morioka Y and Ueda K (1993) Phys. Rev. A **47**, 1187

Jacobs V.L, Davis J and Kepple P.C (1976) Phys. Rev. Lett. **37** 1390

Kaufman V and Humphreys C.J (1969) J. Opt. Soc. Am. **59**, 1614

Keller R. A, Warner B. E, Zalewksi E. F, Dyer P, Engleman R and Palmer B. A (1983) J. De Physique Colloque C **7**, 23

Keller R. A and Zalewski E. F (1982) Appl. Opt. **21**, 3992

Keller R. A, Engleman R. Jr., Zalewksi E. F (1979) Appl. Opt. Soc. Am. **69**, 738

Kellert F. G, Smith K. A, Rundel R. D, Dunning F. B, Kimura and Stebbings R. F (1980) J. Chem. Phys. **72**, 3179

King R. F and Latimer C. J (1982) J. Opt. Soc. Am. **72**, 306

Klar D, Harth K, Ganz J, Kraft T, Ruf M-W, Hotop H, Tsemekhman V, Tseemkhman K and Amusia M. Ya (1992) Z. Phys. D: At. Mol. and Cl. **23** 101

Knight R. D and Wang Liang-guo (1985) J. Opt. Soc. Am. **B2**, 1084

- (1986) J. Opt. Soc. Am. **B3**, 1673

Knight R. D and Wang Liang-guo (1985) Phys. Rev. A **32**, 2751

Kopeika N. S and Rosenbaum J (1976) IEEE Trans. Plasma Sci. Ps **4**, 51

Kopeika N. S (1977) IEEE Trans. Plasma Sci. Ps **6**, 139

Labastie P, Biraben F and Giecobino E (1982) J. Phys. B: At. Mol. Phys. **15**, 2595

Landais J, Huet M, Kucal H and Dohnalik T (1995) J.Phys. B: At. Mol. Opt.Phys.28, 2395

Lawler J. E and Doughtly D. K (1983) J. DE Physique Colleque C **7** 45

Lee C. M and Lu K. T (1975) Phys. Rev. A **8**, 1241

Letokhov V. S and Chebotayev V. P (1977) " Nonlinear Laser Spectroscopy" Vol. 4 Springer-Verlag Berlin Heidelberg New York

Lu K.T (1971) Phys. Rev. **A4**, 579

Lu K. T and Fano U (1970) Phys. Rev. **A2**, 81

Meschede D, Walther H and Müller G (1985) Phys. Rev. Lett. **54** 551

Mizushima (1964) Phys. Rev. A**133**, 414

Moore C.E (1952) " Atomic energy levels" NBS (U.S) Circular No. 467 Vol. **2**

Moore C.E (1958) " Atomic energy levels" NBS (U.S) Circular No. 467 Vol. **3**

Nagvi A.S, Mirza M. Y, Semple D.J and Dulley W.W (1981) Opt. Commun. **37,** 35

Payne m. G, Chen C. H, Hurst G. S, Kramer S. D, Garrett W. R and Pindzola M (1981) Chem. Phys. Lett. **79**, 142

Pellarin M, Vialle J. L, Carre M, Lerme J and Aymar M (1988) J.Phys. B: At. Mol. Opt. Phys. **21**, 383

Penning F.M (1928) Physica **8**, 137

Piracha N. K, Suleman B, Khan S. H and Biag M. A (1995) J. Phys. B: At. Mol. Opt. Phys. **28**, 2525

Piracha N. K, Biag M. A, Khan S. H and Suleman B (1997) J. Phys. B: At. Mol. Opt. Phys. vol. **30**

Radzig A. A and Smirnov B. M (1985) " Reference Data on Atoms, Molecules and Ions " springer series in chemical physic, Springer-Verlag, Berlin.

Racah G (1942) Phys. Rev. **61**, 587

Seaton M.J (1966) Proce. Phys. Soc. **88**, 801

Seaton M. J (1983) Rep. Prog. Phys. **46**, 167

Shuker R, Ben-Amer A, and Erez G (1983) J. DE Physique Colloque C 7 3

Stebbings R. F, Latimer C. J, West W. P, Dunning F. B and Cook T. B (1975) Phys. Rev. A **12**, 1453

Stebbings R. F and Dunning F. B (1983) eds., "Rydberg States of Atoms and Molecules" Cambridge University, U.K

Striganov A.R and Sventitskii N.S (1968) "Tables of Spectral Lines of Neutral and Ionized Atoms" IFI/ Plenum, New York

Turk G.C, Mallard W. G, Schenck P. M and Symith K.C (1979) Analyt. Chem. **51,** 2408

Vasilenko L. S, Chebotaev V. P and Shishaev A. V (1970) JETP Lett. **12,** 113

Ueda K (1987) Phys. Rev. A **35**, 2484

Wang Liang-guo and Knight R. D (1986) Phys. Rev. A **34,** 3902

White H. E (1934) " Introduction to Atomic Spectra" McGraw- Hill Book Company New York.

Wynne J.J and Hermann J.P (1979) Opt. Lett. **4,** 16

Yoon S and Glab W.L (1994) J.Phys. B: At. Mol. Opt. Phys. **27**, 4133

Yoshino K (1970) J. Opt. Soc. Am. **60,** 1220

Yoshino K and Tanaka Y(1979) J. Opt. Soc. Am. **69,** 15

Yoshino K and Freeman D. E (1985) J. Opt. Soc. Am. B **2,** 1268